We did not attempt to optimize the model with respect to the index q, but we did compare results obtained for $q = 1.0$ with those obtained for $q = 1.5$. Figure 4 displays selected 1 minute pitch-angle distributions along with model predictions for the two values of q. The theoretical curves are those implicit in the fits to the time profiles of density and weighted anisotropy in Figure 3; no additional free parameters were introduced in making the comparison shown in Figure 4.

Although the difference is not visually dramatic, we conclude that the $q = 1.0$ fits generally provide a better description of the observations than $q = 1.5$. For the interval 13:56–15:00 UT, $q = 1.0$ provides the better fit for 53 out of 64 available 1 minute samples, as determined by a χ^2 test. Summing over the entire interval, the Fisher F-statistic (Bevington & Robinson 2003) has a value of 1.2994 (ratio of $q = 1.5$ to $q = 1.0$) for 444 degrees of freedom, indicating with 99.7% confidence that $q = 1.0$ yields a significantly better fit. This justifies our use of $q = 1.0$ for modeling the Easter GLE. Further, the radial mean free path and injection onset are not very sensitive to q; with $q = 1.5$ the radial mean free path increases to 0.18 AU, and the injection onset is 1 minute earlier.

4. PARTICLE INJECTION ONSET

One of the key features of Spaceship Earth observations combined with detailed modeling of the data is that injection onset times can be determined with unprecedented precision. (The high particle speed and relatively large mean free paths also contribute.) We conclude that the onset of particle injection onto the Sun-Earth field line was at 13:42 UT ± 1 minute. First detection of particles at Earth was 14 minutes later, implying that the particles traveled a total path length of 1.7 AU in the interplanetary medium. In contrast, that travel time would be ~10 minutes and the path length ~1.2 AU in the case of scatter-free propagation along the spiral magnetic field line. According to our model, scattering by magnetic turbulence in the interplanetary medium is the cause of the extra 0.5 AU in path length and the extra 4 minutes of travel time.

There is now compelling evidence that particles of MeV energies from large gradual solar events (such as the Easter 2001 event) are accelerated by shock waves driven by coronal mass ejections (CMEs; Reames 1999). However, the case for shock acceleration to GeV energies is less firmly established (but see Pomerantz & Duggal 1974 and Levy, Duggal, & Pomerantz 1976). Comparison of the precise injection onset determined from Spaceship Earth with solar radio and optical data reveals clues to the acceleration site and mechanism (cf. Tylka et al. 2002, 2003; Gopalswamy et al. 2002).

An X14.4 soft X-ray event began at 13:11 ST and peaked at 13:42 ST.[3] (Note that in this discussion, we report time of emission at the Sun, which we designate "ST." For electromagnetic radiation, ST is simply the Universal Time of observation minus the 8 minute travel time.) Hard X-rays were emitted starting at 13:28 ST. Hα emission from a flare located at S20 W85 began at 13:28 ST and peaked at 13:41 ST. Type III radio emission[4] due to energetic electrons began at 13:36 ST. Radio burst onsets signifying the formation of a shock wave occurred at 13:40 ST (type II) and 13:44 ST (type IV). CME liftoff is estimated to have occurred between 13:24 ST (linear fit) and 13:31 ST (quadratic fit).[5] From the start of particle injection at 13:42 ST until the end of the interval shown in

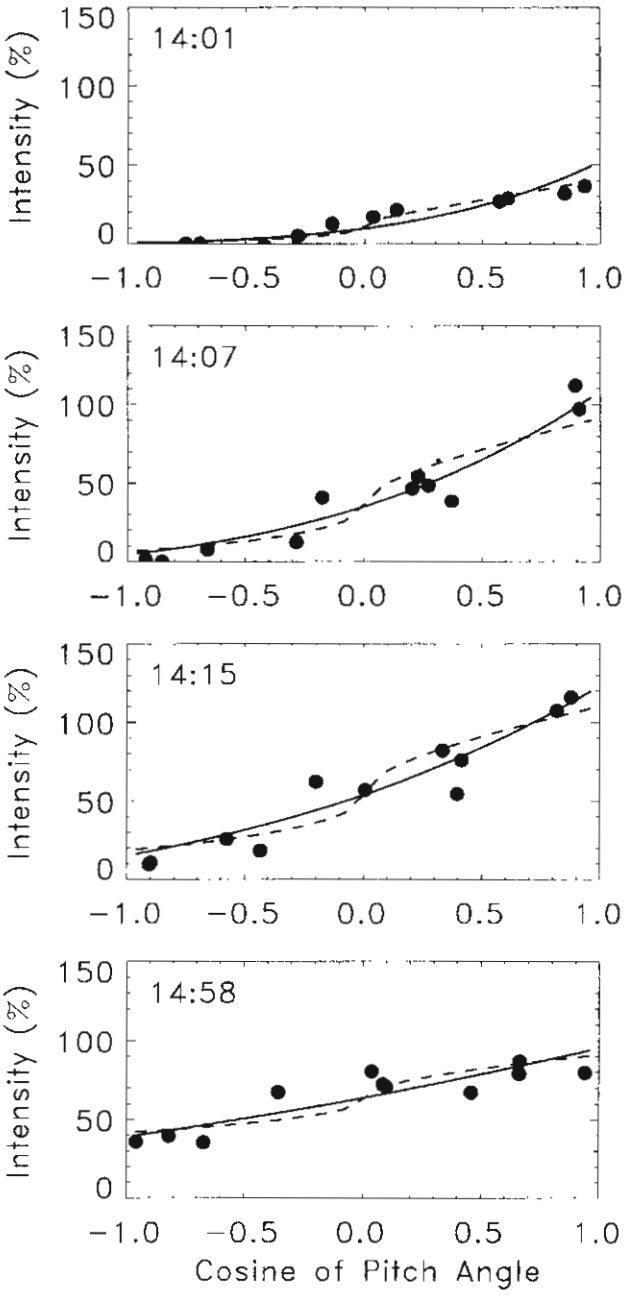

FIG. 4.—Selected 1 minute pitch-angle distributions compared with model predictions for $q = 1.0$ (*solid line*) and $q = 1.5$ (*dashed line*). Each data point represents the intensity recorded by an individual Spaceship Earth station for the UT minute starting at the time shown in the top left of each panel. Pitch angle is the angle between the station asymptotic viewing direction and the symmetry axis determined from the first-order fit to the data.

[3] Timing information for solar radio, optical, and soft X-ray data is available on-line from the Space Environment Center. The URL for the Easter event listing is http://solar.sec.noaa.gov/ftpdir/indices/2001_events/20010415events.txt. Timing information for hard X-rays is from *Yohkoh*/hard X-ray telescope and is available online at http://www.lmsal.com/SXT.

[4] The frequency range of all radio data mentioned here is 30–80 MHz.

[5] Source: *Solar and Heliospheric Observatory* (*SOHO*)/Large Angle and Spectrometric Coronagraph Experiment CME catalog, available on the Web at http://cdaw.gsfc.nasa.gov/CME_list. This CME catalog is generated and maintained by NASA and Catholic University of America in cooperation with the Naval Research Laboratory. *SOHO* is a project of international cooperation between ESA and NASA.

Figure 3, the CME moved from a height of approximately 2 solar radii above the solar surface to approximately 10 solar radii above the solar surface.[6]

5. DISCUSSION

In summary, flare onset in the Easter 2001 event was at 13:11 ST (onset of soft X-ray emission), CME liftoff was between 13:24 and 13:31 ST, and particle injection onset was at 13:42 ST. The particle onset is only 2.6 minutes earlier than that reported by Tylka et al. (2003) using the inverse velocity method, but we believe that our onset is the more reliable because it is based on a more complete treatment of interplanetary transport. Since the CME release and flare onset both preceded the particle injection onset, acceleration in the flare or by a CME shock are both possible sources for the GeV solar particles observed on Easter 2001. Nonetheless, the onset timing would tend to favor shock acceleration, because (1) the particle injection onset is closer in time to the CME liftoff than the flare onset (~15 vs. 31 minutes), and (2) the particle injection onset is accompanied by shock-associated radio signatures.

Our modeling has yielded not only the particle injection onset but also a detailed time profile of the injection process (Fig. 3, *top panel*). The shape of this profile is presumably determined by details of the acceleration process and possible transport processes in the solar corona. Modeling these processes is beyond the scope of this Letter, but we invite researchers in flare acceleration and shock acceleration to attempt to explain this profile with their models.

[6] See figure at http://cdaw.gsfc.nasa.gov/CME_list/UNIVERSAL/2001_04/htpng/20010415.140631.p268g.htp.html.

Our modeling of particle pitch-angle distributions in the Easter event has also provided information on the "q" parameter, which according to scattering theory is linked to the slope of the magnetic power spectrum (Jokipii 1966). Specifically we found that a value $q = 1$ provides a better fit to the data than $q = 1.5$. This is somewhat surprising, because 2 GV particles are typically resonant with the low end of the turbulence inertial range, where a slope near the Kolmogoroff value, $q = 5/3$, might be expected. [Specifically, the resonant wavenumber is $k_{res} = (R_L \cos\theta)^{-1}$, where R_L and θ are the particle Larmor radius and pitch angle. In this event, we estimate $k_{res} > 10^{-6}$ km^{-1}, whereas the inertial range would typically begin at 5 times lower wavenumber, $k = 2 \times 10^{-7}$ km^{-1}.] Indeed, pitch-angle distributions in the Bastille Day event do exhibit a rapid variation near 90° pitch angle, which is characteristic of the higher q values (see Fig. 12 of Bieber et al. 2002).

However, a preliminary analysis of *Wind* Magnetic Fields Investigation magnetic field data for the Easter event does reveal an unusual spectral break at $k = 10^{-5}$ km^{-1}, with a spectral index of $q = 1.3$ below and $q = 1.8$ above this value. This is qualitatively in accord with our result of a low q-value in the Easter event.

We thank R. Schwenn for a useful discussion. We thank our colleagues at IZMIRAN (Russia), Polar Geophysical Institute (Russia), and Australian Antarctic Division for furnishing data. This work was supported by the US National Science Foundation under grant ATM-0000315, by the Thailand Research Fund, and by the Rachadapisek Sompoj Fund of Chulalongkorn University.

REFERENCES

Bevington, P. R., & Robinson, D. K. 2003, Data Reduction and Error Analysis for the Physical Sciences (3d ed.; Boston: McGraw Hill)
Bieber, J. W., Chen, J., Matthaeus, W. H., Smith, C. W., & Pomerantz, M. A. 1993, J. Geophys. Res., 98, 3585
Bieber, J. W., & Pomerantz, M. A. 1983, Geophys. Res. Lett., 10, 920
Bieber, J. W., et al. 2002, ApJ, 567, 622
Gopalswamy, N., Yashiro, S., Kaiser, M. L., & Howard, R. A. 2002, Adv. Space Res., in press
Jokipii, J. R. 1966, ApJ, 146, 480
Levy, E. H., Duggal, S. P., & Pomerantz, M. A. 1976, J. Geophys. Res., 81, 51
Lin, Z., Bieber, J. W., & Evenson, P. 1995, J. Geophys. Res., 100, 23,543
Matthaeus, W. H., & Goldstein, M. L. 1982, Phys. Rev. Lett., 57, 495
Pomerantz, M. A., & Duggal, S. P. 1974, J. Geophys. Res., 79, 913
Reames, D. V. 1999, Space Sci. Rev., 90, 413
Roelof, E. C. 1969, in Lectures in High Energy Astrophysics, ed. H. Ögelmann & J. R. Wayland (NASA SP-199; Washington, DC: NASA), 111
Ruffolo, D. 1995, ApJ, 442, 861
Ruffolo, D., Khumlumlert, T., & Youngdee, W. 1998, J. Geophys. Res., 103, 20,591
Tylka, A. J., Boberg, P. R., Cohen, C. M. S., Dietrich, W. F., Maclennan, C. G., Mason, G. M., Ng, C. K., & Reames, D. V. 2002, ApJ, 581, L119
Tylka, A. J., et al. 2003, Proc. 28th Int. Cosmic Ray Conf. (Tsukuba), 3305

The Astrophysical Journal, 614:420–434, 2004 October 10

SEPARATION OF MAGNETIC FIELD LINES IN TWO-COMPONENT TURBULENCE

D. Ruffolo,[1,2] W. H. Matthaeus,[3] and P. Chuychai[1,3]
Received 2002 December 24; accepted 2004 June 18

ABSTRACT

The problem of the separation of random magnetic field lines in collisionless astrophysical plasmas is closely related to the problem of the magnetic field line random walk and is highly relevant to the transport of charged particles in turbulent plasmas. In order to generalize treatments based on quasi-linear theory, here we examine the separation of nearby magnetic field lines by employing a nonperturbative technique based on the Corrsin independence hypothesis. Specifically, we consider the case of two-component turbulence in which the magnetic field fluctuations are a mixture of one-dimensional (slab) and two-dimensional ingredients, as a concrete example of anisotropic turbulence that provides a useful description of turbulence in the solar wind. We find that random field trajectories can separate in general through three regimes of the behavior of the running diffusion coefficient: slow diffusive separation, an intermediate regime of superdiffusion, and fast diffusive separation at large distances. These features are associated with the gradual, exponential divergence of field lines within islands of two-dimensional turbulence, followed by diffusive separation at long distances. The types of behavior are determined not by the Kubo number but rather a related ratio that takes the turbulence anisotropy into account. These results are confirmed by computer simulations. We discuss implications for space observations of energetic charged particles, including "dropouts" of solar energetic particles.

Subject headings: diffusion — magnetic fields — Sun: particle emission — turbulence

1. INTRODUCTION

The random walk of individual magnetic field lines relative to the mean magnetic field and the rate of separation of nearby field lines are key issues in defining the topology and structure of random magnetic fields in magnetohydrodynamic (MHD) turbulence. The statistics of such a random walk are often central to understanding the diffusion of energetic charged particles perpendicular to the mean magnetic field in astrophysical plasmas (Jokipii 1966; Jokipii & Parker 1968). Perpendicular diffusion is an important component of the solar cycle–dependent modulation of Galactic cosmic rays (Parker 1965; Moraal 1976; Cane et al. 1999; Reinecke et al. 2000). Determining the rate of perpendicular diffusion of energetic particles in the heliosphere may be crucial in distinguishing between two popular models for explaining the dramatic observations by the *Ulysses* spacecraft of apparent corotating interaction region (CIR) modulation of Galactic and anomalous cosmic rays (Kunow et al. 1995; McKibben et al. 1995; Simpson et al. 1995) and acceleration of low-energy electrons and ions (Sanderson et al. 1995; Simnett et al. 1995) at higher heliospheric latitudes than where CIRs were observed, i.e., the models of Kóta & Jokipii (1995) and Fisk (1996). Other issues of energetic particle transport in the heliosphere may rely on details of perpendicular diffusion, such as the poor access of Galactic cosmic rays into a coronal mass ejection (Cane et al. 1994) that can account for the deep minima of Forbush decreases, or energetic particle acceleration at a nearly perpendicular shock (Jokipii 1987; Jokipii et al. 1993; Kirk et al. 1996; Jones et al. 1998).

On the other hand, there are also situations in which the behavior of distributions of energetic charged particles might be better understood in terms of the mutual separation of field lines than by the random walk of individual field lines (Jokipii 1973). Indeed, for an initially concentrated distribution of particles (assumed to be following field lines) to spread in the directions perpendicular to the mean magnetic field requires that the field lines threading the distribution mutually separate; a correlated wandering of nearby field lines would just displace the particle distribution without distorting it. Figure 1 illustrates the random walk perpendicular to the mean field (Δx), the displacement between nearby field lines ($X \equiv x_2 - x_1$), and their separation $\Delta X \equiv X - X_0$. In the extreme case in which two turbulent field lines are completely decorrelated, the mean squared separation would be twice the mean squared random walk. On the other hand, two nearby field lines could follow highly correlated trajectories with a mutual separation much lower than the displacement from the mean field, as represented by the lower two field lines in Figure 1. Therefore, field line separation is a sensitive probe of the dissimilarity of nearby field lines and the transverse structure of magnetic turbulence.

One application of calculating the field line separation is to address the long-recognized phenomenon of "channeling," or sudden changes in the fluxes of solar energetic particles (SEPs), which has been revisited by recent, detailed measurements of Mazur et al. (2000), who refer to such events as "dropouts." These are presumably due to sudden changes in magnetic connection to a spatially localized injection region. This picture requires that field lines that are adjacent when near the Sun remain confined to localized flux tubes out to distances $\sim$1 AU along the mean field.

In particular, Mazur et al. (2000) identify episodes of dramatic SEP intensity changes on an average timescale of 3 hr,

[1] Department of Physics, Chulalongkorn University, Bangkok 10330, Thailand; david_ruffolo@yahoo.com, piyanate@corona.phys.sc.chula.ac.th.
[2] Current address: Department of Physics, Faculty of Science, Mahidol University, Rama VI Road, Bangkok 10400, Thailand.
[3] Bartol Research Institute, University of Delaware, Newark, DE 19716; yswhm@bartol.udel.edu.

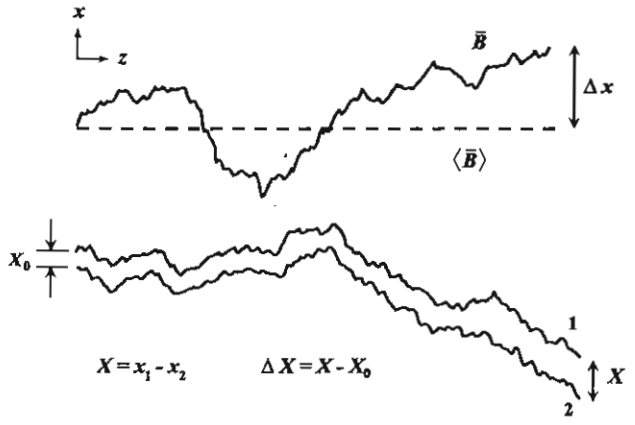

FIG. 1. Illustration of the magnetic field line random walk perpendicular to the mean field (Δx), displacement between nearby field lines ($X \equiv x_2 - x_1$), and their separation ($\Delta X \equiv X - X_0$). The present work calculates the mean squared separation vs. distance along the mean field.

corresponding to a spatial (longitudinal) scale of 0.03 AU. Giacalone et al. (2000) point out that if there is effectively no turbulent random walk, one can understand dropouts in terms of the field line random walk due to photospheric motions. This leads to the question, Why is there no apparent turbulent random walk? There certainly is turbulence in the interplanetary medium. One might expect a longitudinal diffusion of field lines (due to the two-dimensional component of solar wind fluctuations) to a scale of $(\Delta x)_{\rm rms} \sim (2D_\perp \Delta z)^{1/2}$, where the diffusion coefficient of the turbulent random walk is $D_\perp = (b/B_0)(\tilde{\lambda}/\sqrt{2})$ (Matthaeus et al. 1995) and $\tilde{\lambda}$ is the "ultrascale" or "mesoscale," inferred from observations to be ~0.2 AU (Matthaeus et al. 1999). For a typical rms turbulent magnetic field of one-half the mean field, $b = 0.5B_0$, the expected longitudinal scale of the turbulent random walk is 0.37 AU, which would wash out the observed dropouts. One possible explanation might be that the separation of nearby field lines, which controls the spread of particles from a small injection region near the Sun, could be much slower than the turbulent random walk relative to the mean field, as illustrated in Figure 1. This issue, which is discussed again in § 6, is just one example of an astrophysical problem related to the separation of nearby magnetic field lines.

The theory of the separation of adjacent field lines has been examined by Jokipii (1973) and Zimbardo et al. (1984). This issue has been recognized as relevant to physical processes in fusion plasmas (e.g., Rechester & Rosenbluth 1978; Kadomtsev & Pogutse 1979; Isichenko 1991a, 1991b), the solar corona (e.g., Similon & Sudan 1989), energetic particle transport in the heliosphere (Erdős et al. 1997, 1999), cosmic-ray transport and acceleration in the Galaxy (Barge et al. 1984; Chandran 2000), and thermal conduction in galaxy clusters (Maron et al. 2004). Much attention has been devoted in the past to description of the exponential separation of field lines (Rechester & Rosenbluth 1978; Kadomtsev & Pogutse 1979) in the regime of small separation before the field lines undergo independent random walks, because of the relationship of that phenomenon to mixing in ergodic theory (Zaslavsky & Chirikov 1972) and stochastic instability in general. In the present paper we are mainly concerned with regimes of diffusive behavior, although we comment on the relationship between these two views of field line separation. The length scale along the mean field over which field lines separate by a perpendicular coherence scale is relevant to incompressible MHD turbulence (Goldreich & Sridhar 1997; Lithwick & Goldreich 2001).

Apart from the observational issues discussed above, there are also a number of theoretical issues that provide motivation for reconsidering field line separation in a "realistic" (or, at least, observationally motivated) three-dimensional model magnetic field. For example, one feature of turbulence structure that has become recognized in recent years (Jones et al. 1998) is that models that are one-dimensional ("slab") or that admit even one ignorable coordinate give rise to pathological statistical representations of particle transport. There are also indications that the stochastic instability of field lines has a character in models having small numbers of coherent modes that contrasts strongly with its character in a continuum of incoherent modes (Rax & White 1992). It is reasonable to anticipate that such differences would affect the onset and nature of diffusion. One is cautioned, then, that some properties that emerge from the simpler models of field line separation should not be taken as rigorous, especially in the light of better understood properties from observations and turbulence simulations. An example is the rather general identification of the correlation scale with the exponential separation scale (e.g., Sagdeev et al. 1988), although this is not a well-understood relationship (Rechester & Rosenbluth 1978). Similarly, the identification of the correlation scale of magnetic fluctuations with the correlation scale of the *spatial gradients* of the fluctuations (Isichenko 1991a) is manifestly incorrect for turbulence having distinct inner and outer scales. Moreover, for homogeneous turbulence, the correlation scale of derivatives, i.e., the Taylor microscale, may differ from the fluctuation correlation scale by orders of magnitude (Batchelor 1953). This difference is at least 3 or 4 orders of magnitude in the solar wind (Matthaeus & Goldstein 1982). Finally, we note that the realm of applicability of the perturbative quasi-linear (QLT) limit is often expressed (Isichenko 1991a) in terms of a dimensionless (Kubo) number $R = (b/B_0)(\lambda_\parallel/\lambda_\perp)$, where $\lambda_\parallel$ and $\lambda_\perp$ are, respectively, correlation scales in the directions parallel to and perpendicular to the large-scale mean magnetic field B_0. QLT is supposed to be accurate when $R \ll 1$. While qualitatively correct, we can see that a criterion based solely on R cannot be complete, in view of the fact that the contribution to field line diffusion due to a quasi-two-dimensional component of the turbulence (Matthaeus et al. 1995) depends on not $\lambda_\perp$ but a distinct scale (the "ultrascale"; see below) that characterizes large-scale transverse magnetic structure.

In the following sections we reexamine the theory of the separation of adjacent field lines in astrophysical MHD turbulence in light of improved understanding of solar wind turbulence in recent years (Matthaeus et al. 1990; Bieber et al. 1994). We consider field line separation in two-component turbulence consisting of a slab component that varies only along the mean field, as well as a two-dimensional component that varies only in the two transverse directions, which has been shown to serve as a useful model of solar wind turbulence (Bieber et al. 1996). This turbulence model can also be viewed as a concrete example that is representative of anisotropic turbulence in general, i.e., turbulence that varies differently along or perpendicular to the mean magnetic field. We proceed using a nonperturbative approach similar to that which has been used previously (Matthaeus et al. 1995; Gray

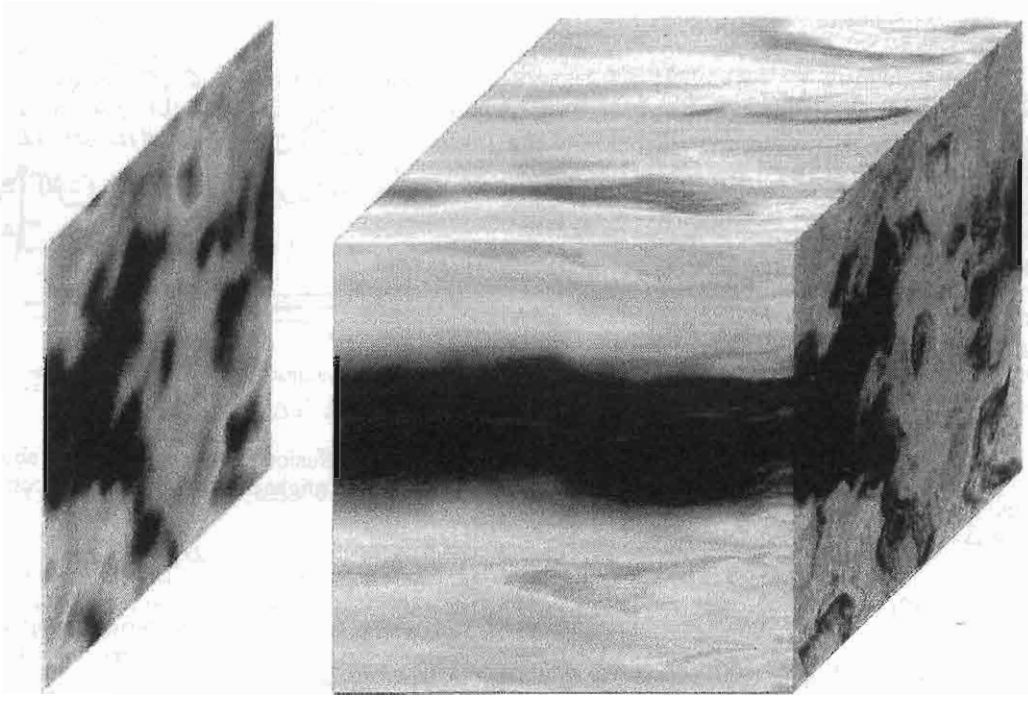

FIG. 2.—Field line motion in a realization of 2D+slab turbulence. In the left part of the figure, the shading indicates the initial value of $a(x,y)$, the potential function for the two-dimensional component. In the right part, that initial shading is convected along random field lines. The mean field direction, $\hat{z}$, is to the right. It can be seen that some regions exhibit strong mixing, while others are still organized as distinct flux tubes.

et al. 1996) to examine the field line random walk. The analytic results are verified by computer simulations. We then consider their astrophysical implications.

2. 2D+SLAB TURBULENCE

In the 2D+slab model of magnetic turbulence, we assume

$$\boldsymbol{B} = \boldsymbol{B}_0 + \boldsymbol{b}(x,y,z), \tag{1}$$

where the mean field $\boldsymbol{B}_0$ is constant. We also use

$$\boldsymbol{B}_0 = B_0\hat{z}, \quad \boldsymbol{b} \perp \hat{z}, \tag{2}$$

and the fluctuating field, of mean zero, is given by

$$\boldsymbol{b} = \boldsymbol{b}^{2D}(x,y) + \boldsymbol{b}^{\rm slab}(z). \tag{3}$$

For brevity, we refer to a quantity such as $\langle b^2\rangle$ as the magnetic energy of the fluctuations. In general, we can write

$$\boldsymbol{b}^{2D}(x,y) = \nabla\times[a(x,y)\hat{z}]. \tag{4}$$

where $a\hat{z}$ can be interpreted as a vector potential for the two-dimensional component of turbulence or as a poloidal (transverse) flux function, in the sense that $\int_1^2 \boldsymbol{b}^{2D}\cdot\hat{\boldsymbol{n}}\,d\ell = a(2) - a(1)$, where $d\ell$ is the line element along any curve connecting points 1 and 2 and $\hat{\boldsymbol{n}}$ is the two-dimensional normal to that curve. Note that any large-scale gradient in a would violate the assumption that the mean magnetic field is uniform and along the $\hat{z}$-direction. Thus, $a(x,y)$ can be viewed as a random function, fluctuating about a constant mean value, taken to be zero for convenience, with a well-behaved power spectrum $A(k_x,k_y)$.

This form of magnetic turbulence was motivated by an analysis of magnetic fluctuations in the solar wind (Matthaeus et al. 1990). Note that with $\boldsymbol{b}\perp\hat{z}$, we have $B_z \equiv B_0$, so in this model it is impossible for a magnetic field line to backtrack in the z-direction, and the z-coordinate uniquely specifies a point on a magnetic field line. This permits a direct analogy between the perpendicular motion of a magnetic field line versus z and the trajectory of a fluid element in incompressible, two-dimensional fluid dynamics versus time.

Figure 2 illustrates the flux function $a(x,y)$ and the motion of field lines for a realization of such 2D+slab turbulence with an 80 : 20 ratio of two-dimensional to slab component energies, as found in the solar wind (Bieber et al. 1994, 1996). In the absence of a slab component, the 2D-turbulent field lines would move along curves of constant a, since equation (4) indicates that $\boldsymbol{b}^{2D}\perp\nabla a$. (This is analogous to Hamiltonian flow, upon the substitutions $a\to H$ and $z\to t$.) In three dimensions, such field lines are constrained to flux tubes that are "cylinders" in the mathematical sense of surfaces of constant $a(x,y)$. What makes 2D+slab turbulence interesting is that the slab component imposes random perturbations on the field line motion, leading to mixing of field lines and wandering to regions of different $a(x,y)$ (see also Matthaeus et al. 1995). This is illustrated in Figure 2, where the left panel shows an initial shading according to a realization of $a(x,y)$ and the right panel shows how that shading is convected along random field lines (the distance z along the mean field increases to the right). In the absence of slab turbulence, the shading would be constant with z as field lines stick to the same value of a. In contrast, Figure 2 illustrates how the slab turbulence "mixes" field lines of different initial a-values. It is interesting that some regions exhibit strong mixing and spreading, while in others the initial shading is clearly visible in the same location, indicating that a flux tube structure is maintained over this

distance, a phenomenon that is discussed further by Ruffolo et al. (2003).

3. RANDOM WALK OF A SINGLE FIELD LINE

It is instructive to first review the diffusive random walk of a single magnetic field line in the 2D+slab model of turbulence. While yielding the same result as Matthaeus et al. (1995) in the long-distance limit, the present calculation allows us to determine its range of applicability and employs a different form of Corrsin's hypothesis, which we also use in the calculation of field line separation.

Following Jokipii & Parker (1969) and Jokipii (1973), we start with the defining equation of a magnetic field line,

$$\frac{dx}{B_x} = \frac{dy}{B_y} = \frac{dz}{B_z}, \tag{5}$$

and express the change in, say, the x-coordinate of a field line over a distance Δz along the mean magnetic field as

$$\Delta x \equiv x(\Delta z) - x(0) = \frac{1}{B_0}\int_0^{\Delta z} b_x[x(z'), y(z'), z']\, dz'. \tag{6}$$

This quantity is illustrated in Figure 1. The ensemble average of $(\Delta x)^2$ is then given by

$$\begin{aligned}\langle \Delta x^2 \rangle &= \frac{1}{B_0^2}\int_0^{\Delta z}\int_0^{\Delta z} \langle b_x[x(z'), y(z'), z'] \\ &\qquad \times b_x[x(z''), y(z''), z'']\rangle\, dz'\, dz'' \\ &= \frac{1}{B_0^2}\int_0^{\Delta z}\int_0^{\Delta z} \langle b_x(x', y', z') b_x(x'', y'', z'')\rangle\, dz'\, dz'', \end{aligned} \tag{7}$$

where we introduce the notation x' for $x(z')$, etc. We can also write

$$\begin{aligned}\langle \Delta x^2 \rangle &= \frac{1}{B_0^2}\int_0^{\Delta z}\int_{-z'}^{\Delta z - z'} \langle b_x(x', y', z') \\ &\qquad \times b_x(x'', y'', z' + \Delta z')\rangle\, d\Delta z'\, dz', \end{aligned} \tag{8}$$

where $\Delta z' \equiv z'' - z'$, and with the assumption of homogeneity,

$$\begin{aligned}\langle \Delta x^2 \rangle &= \frac{1}{B_0^2}\int_0^{\Delta z}\int_{-z'}^{\Delta z - z'} \langle b_x(0, 0, 0) \\ &\qquad \times b_x(\Delta x', \Delta y', \Delta z')\rangle\, d\Delta z'\, dz', \end{aligned} \tag{9}$$

where $\Delta x' \equiv x'' - x'$ and $\Delta y' \equiv y'' - y'$. This equation describes the random walk of a single field line, and the quantities z', z'', $\Delta z'$, and $\Delta x'$ are illustrated in Figure 3.

Before proceeding further with the mathematical derivation, it is interesting to motivate the Matthaeus et al. (1995) result. Physically, a random walk should give diffusive behavior, with

$$\langle \Delta x^2 \rangle = 2D_\perp \Delta z, \tag{10}$$

$$D_\perp \sim \left\langle (dx/dz)^2 \right\rangle \ell \sim \frac{\langle b_x^2 \rangle}{B_0^2}\ell, \tag{11}$$

for a "mean free distance" ℓ. In terms of equation (9), b_x at z' and z'' decorrelate over some distance $\Delta z' \sim \ell$, so the inner integral is of order $2\langle b_x^2\rangle \ell$, the outer integral of order $2\langle b_x^2\rangle \ell \Delta z$,

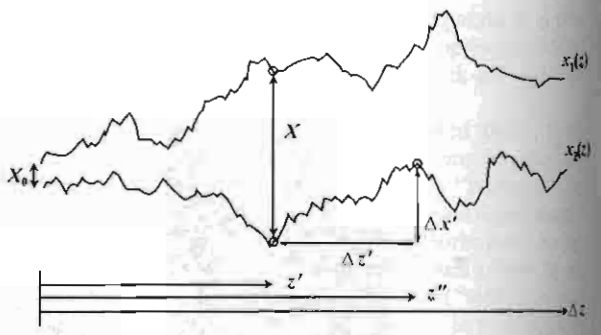

FIG. 3.—Schematic of two random field lines and definition of various quantities.

and the diffusion coefficient as given above. For slab turbulence, one might estimate ℓ to be the correlation length ℓ_c:

$$D_\perp^{\rm slab} \sim \frac{\langle b_x^2 \rangle}{B_0^2}\ell_c, \tag{12}$$

a well-known result to be derived shortly in detail. For two-dimensional turbulence, decorrelation takes place for $\langle \Delta x^2 \rangle \sim \tilde{\lambda}^2$, at some perpendicular distance $\tilde{\lambda}$, which Matthaeus et al. (1995) refer to as the "ultrascale" (to be precisely defined later, in eq. [37]). Then

$$\ell \sim \frac{\tilde{\lambda}^2}{2D_\perp}, \quad D_\perp \sim \frac{\langle b^2 \rangle}{B_0^2}\frac{\tilde{\lambda}^2}{2D_\perp} \tag{13}$$

which has an interesting implicit form. This leads to

$$D_\perp^{\rm 2D} \sim \frac{\tilde{\lambda}}{\sqrt{2}}\frac{\sqrt{\langle b^2 \rangle}}{B_0}, \tag{14}$$

which depends on the rms level of fluctuation instead of the mean square. From the detailed mathematical derivation, it is seen that the ultrascale $\tilde{\lambda}$ can be identified with the mean squared fluctuation of $a(x, y)$ divided by that of $b^{\rm 2D}(x, y)$. Note that this result (eq. [14]) refers to two-component turbulence in the limit of vanishing slab fluctuations. This limit is singular because for pure two-dimensional turbulence, field lines on closed flux surfaces remain confined and formally do not undergo diffusion.

Continuing with the derivation, note that Lagrangian correlation functions such as $\langle b_x(x', y', z') b_x(x'', y'', z'')\rangle$ differ from standard (Eulerian) correlation functions; in a Lagrangian ensemble average over representations of the magnetic turbulence, the positions themselves depend on the representation. However, it is possible to separate the statistics of the magnetic fluctuations from those of individual trajectories when the two positions are displaced by more than a coherence length in the parallel or perpendicular direction. (Over smaller distances this is not necessarily accurate, e.g., straight line trajectories, with one spatial distribution, are associated with higher magnetic correlation than bending trajectories, which have a different spatial distribution.) This approximation, known as Corrsin's independence hypothesis (Corrsin 1959; Salu & Montgomery 1977; see also McComb 1990) can be expressed either in wavevector space (as in Matthaeus et al. 1995) or in position space. Computer simulations have been used to verify the hypothesis for the random walk calculation (Gray et al. 1996) and are also used to verify its validity in the present work.

Here we demonstrate the implementation of Corrsin's hypothesis in position space. We consider the Lagrangian correlation function to be the Eulerian correlation function, $R_{xx} \equiv \langle b_x(0,0,0) b_x(x,y,z)\rangle$, weighted by the conditional probabilities of finding $\Delta x'$ and $\Delta y'$ after a given $\Delta z'$:

$$\langle b_x(0,0,0) b_x(\Delta x'(\Delta z'), \Delta y'(\Delta z'), \Delta z')\rangle = \int_{-\infty}^{\infty}\int_{-\infty}^{\infty} R_{xx}(\Delta x', \Delta y', \Delta z') \times P(\Delta x'|\Delta z') P(\Delta y'|\Delta z')\, d\Delta x'\, d\Delta y', \tag{15}$$

$$\langle \Delta x^2\rangle = \frac{1}{B_0^2}\int_0^{\Delta z}\int_{-z'}^{\Delta z - z'}\int_{-\infty}^{\infty}\int_{-\infty}^{\infty} R_{xx}(\Delta x', \Delta y', \Delta z') \times P(\Delta x'|\Delta z') P(\Delta y'|\Delta z')\, d\Delta x'\, d\Delta y'\, d\Delta z'\, dz', \tag{16}$$

where we invoke the statistical independence of $\Delta x'$ and $\Delta y'$.

Another key assumption is that the conditional probability distributions are Gaussian,

$$P(\Delta x'|\Delta z') = \frac{1}{\sqrt{2\pi\sigma_x^2}} \exp\left[-\frac{(\Delta x')^2}{2\sigma_x^2}\right],$$
$$P(\Delta y'|\Delta z') = \frac{1}{\sqrt{2\pi\sigma_y^2}} \exp\left[-\frac{(\Delta y')^2}{2\sigma_y^2}\right]. \tag{17}$$

Furthermore, we assume that the variances $\sigma_x^2 = \langle \Delta x^2\rangle$ and $\sigma_y^2 = \langle \Delta y^2\rangle$ are diffusive and statistically axisymmetric in the sense that

$$\langle \Delta x^2\rangle = \langle \Delta y^2\rangle = 2D_\perp |\Delta z'|, \tag{18}$$

where $D_\perp$ is the desired perpendicular diffusion coefficient. The distributions in equation (17) guarantee the statistical independence assumed in equation (16). For slab or two-component turbulence, these assumptions are accurate for sufficiently large Δz, by the central limit theorem. A check on the validity of the result is that $\langle \Delta x^2\rangle$ should be proportional to Δz in that limit, and as Δz decreases, violation of that proportionality indicates the limit of validity of the diffusion approximation. For example, at small Δz, over which $\boldsymbol{b}$ is nearly constant, there is a "free-streaming" regime in which field lines have nearly straight-line trajectories and $\langle \Delta x^2\rangle \propto (\Delta z)^2$.

So far, our calculation of $\langle \Delta x^2\rangle$ has not yet specified the nature of the magnetic turbulence. Now let us focus on axisymmetric, two-component 2D+slab turbulence (eqs. [1]–[3]):

$$R_{xx}(\Delta x', \Delta y', \Delta z') = R_{xx}^{\rm slab}(\Delta z') + R_{xx}^{\rm 2D}(\Delta x', \Delta y'), \tag{19}$$

or in terms of power spectra,

$$R_{xx}^{\rm slab}(\Delta z') = \frac{1}{\sqrt{2\pi}}\int_{-\infty}^{\infty} P_{xx}^{\rm slab}(k_z) e^{ik_z \Delta z'}\, dk_z,$$
$$R_{xx}^{\rm 2D}(\Delta x', \Delta y') = \frac{1}{2\pi}\int_{-\infty}^{\infty}\int_{-\infty}^{\infty} P_{xx}^{\rm 2D}(k_x, k_y) e^{-ik_x \Delta x'} \times e^{-ik_y \Delta y'}\, dk_x\, dk_y. \tag{20}$$

Then, substituting equations (19) and (20) into equation (16) and separating slab and two-dimensional contributions, we have

$$\langle \Delta x^2\rangle_{\rm slab} = \frac{1}{\sqrt{2\pi}}\frac{1}{B_0^2}\int_{-\infty}^{\infty} P_{xx}^{\rm slab}(k_z)\int_0^{\Delta z}\int_{-z'}^{\Delta z - z'}\left[\int_{-\infty}^{\infty} P(\Delta x'|\Delta z')\, d\Delta x'\right] \times \left[\int_{-\infty}^{\infty} P(\Delta y'|\Delta z')\, d\Delta y'\right] e^{-ik_z \Delta z'}\, d\Delta z'\, dz'\, dk_z, \tag{21}$$

$$\langle \Delta x^2\rangle_{\rm 2D} = \frac{1}{2\pi}\frac{1}{B_0^2}\int_{-\infty}^{\infty}\int_{-\infty}^{\infty} P_{xx}^{\rm 2D}(k_x, k_y) \times \int_0^{\Delta z}\int_{-z'}^{\Delta z - z'}\left[\int_{-\infty}^{\infty} e^{-ik_x \Delta x'} P(\Delta x'|\Delta z')\, d\Delta x'\right] \times \left[\int_{-\infty}^{\infty} e^{-ik_y \Delta y'} P(\Delta y'|\Delta z')\, d\Delta y'\right] d\Delta z'\, dz'\, dk_x\, dk_y. \tag{22}$$

For the slab component of turbulence, in which $R_{xx}^{\rm slab}$ does not depend on $\Delta x'$ or $\Delta y'$, the conditional probabilities simply integrate to 1, yielding

$$\langle \Delta x^2\rangle_{\rm slab} = \frac{1}{\sqrt{2\pi}}\frac{1}{B_0^2} \times \int_{-\infty}^{\infty}\int_0^{\Delta z}\int_{-z'}^{\Delta z - z'} P_{xx}^{\rm slab}(k_z) e^{-ik_z \Delta z'}\, d\Delta z'\, dz'\, dk_z. \tag{23}$$

For the two-dimensional component, we have

$$\int_{-\infty}^{\infty} e^{-ik_x \Delta x'} P(\Delta x'|\Delta z')\, d\Delta x' = \int_{-\infty}^{\infty} \frac{e^{-ik_x \Delta x'}}{\sqrt{4\pi D_\perp |\Delta z'|}} \exp\left[-\frac{(\Delta x')^2}{4D_\perp |\Delta z'|}\right] d\Delta x' = e^{-D_\perp k_x^2 |\Delta z'|}, \tag{24}$$

and with the analogous formula for the $\Delta y'$ integral, we obtain

$$\langle \Delta x^2\rangle_{\rm 2D} = \frac{1}{2\pi}\frac{1}{B_0^2}\int_{-\infty}^{\infty}\int_{-\infty}^{\infty}\int_0^{\Delta z}\int_{-z'}^{\Delta z - z'} P_{xx}^{\rm 2D}(k_x, k_y) \times e^{-D_\perp (k_x^2 + k_y^2)|\Delta z'|}\, d\Delta z'\, dz'\, dk_x\, dk_y. \tag{25}$$

So far this derivation is equivalent to that of Matthaeus et al. (1995), except that we consider the exact limits of the $\Delta z'$ integration, not approximating the limits as $\pm\infty$.

Now we may carry out the integration over $\Delta z'$ and z' in equations (23) and (25), to obtain

$$\langle \Delta x^2\rangle_{\rm slab} = \frac{1}{\sqrt{2\pi}}\frac{1}{B_0^2}\int_{-\infty}^{\infty} \frac{2[1 - \cos(k_z \Delta z)]}{k_z^2} P_{xx}^{\rm slab}(k_z)\, dk_z, \tag{26}$$

$$\langle \Delta x^2\rangle_{\rm 2D} = \frac{1}{2\pi}\frac{1}{B_0^2}\int_{-\infty}^{\infty}\int_{-\infty}^{\infty} \frac{2\Delta z P_{xx}^{\rm 2D}(k_x, k_y)}{D_\perp (k_x^2 + k_y^2)} \times \left[1 + \frac{e^{-D_\perp (k_x^2 + k_y^2)\Delta z} - 1}{D_\perp (k_x^2 + k_y^2)\Delta z}\right] dk_x\, dk_y = \frac{1}{2\pi}\frac{1}{B_0^2}\frac{2\Delta z}{D_\perp}\int_{-\infty}^{\infty}\int_{-\infty}^{\infty} \frac{P_{xx}^{\rm 2D}(k_x, k_y)}{k_\perp^2} \times \left[1 - g(D_\perp k_\perp^2 \Delta z)\right] dk_x\, dk_y, \tag{27}$$

where $k_\perp^2 \equiv k_x^2 + k_y^2$, and $g(u) \equiv (1 - e^{-u})/u$ behaves as a low-pass filter; i.e., $g(u) \approx 1$ for $u \ll 1$ and monotonically declines to zero as $u \to \infty$. We then obtain an expression for the perpendicular diffusion coefficient for a single field line, $D_\perp \equiv \langle \Delta x^2 \rangle / (2\Delta z)$:

$$D_\perp = \frac{1}{\sqrt{2\pi}} \frac{1}{B_0^2} \int_{-\infty}^{\infty} \frac{[1 - \cos(k_z \Delta z)]}{k_z^2 \Delta z} P_{xx}^{\rm slab}(k_z)\, dk_z + \frac{1}{2\pi} \frac{1}{B_0^2} \frac{1}{D_\perp} \times \int_{-\infty}^{\infty}\int_{-\infty}^{\infty} \frac{P_{xx}^{\rm 2D}(k_x, k_y)}{k_\perp^2} \left[1 - g(D_\perp k_\perp^2 \Delta z)\right] dk_x\, dk_y. \quad (28)$$

Note that this formula is implicit in the sense that $D_\perp$ appears on both sides of the equation and nonperturbative in the sense that it applies for any $P_{xx}^{\rm slab}$ and $P_{xx}^{\rm 2D}$. Note also that a diffusion coefficient is a valid concept only when $\langle \Delta x^2 \rangle \propto \Delta z$, i.e., when this expression for $D_\perp$ is constant in Δz. Next, we show that this is indeed the case for sufficiently large Δz.

Equation (28) can be interpreted further when we consider that most observed power spectra of magnetic turbulence have power concentrated below and in the vicinity of a certain scale k_0, which is associated with a coherence scale $\ell = 1/k_0$. Now if there is no two-dimensional component, we have

$$D_\perp^{\rm slab} = \frac{1}{\sqrt{2\pi}} \frac{1}{B_0^2} \int_{-\infty}^{\infty} \frac{[1 - \cos(k_z \Delta z)]}{k_z^2 \Delta z} P_{xx}^{\rm slab}(k_z)\, dk_z. \quad (29)$$

Note that as $\Delta z \to \infty$,

$$\frac{1 - \cos(k_z \Delta z)}{k_z^2 \Delta z} \to \pi \delta(k_z) \quad (30)$$

and

$$D_\perp^{\rm slab} = \sqrt{\frac{\pi}{2}} \frac{P_{xx}^{\rm slab}(0)}{B_0^2}. \quad (31)$$

This dependence, originally derived by Jokipii & Parker (1968), is approximately true for large Δz, i.e., $\Delta z \gg \ell_z = 1/k_{0z}$, where ℓ_z is a parallel coherence length, provided that $P_{xx}^{\rm slab}$ is roughly constant for $k_z \ll k_{0z}$. Equation (31) can also be expressed as

$$D_\perp^{\rm slab} = \frac{\langle b_x^2 \rangle^{\rm slab}}{B_0^2} \ell_c \quad (32)$$

for the correlation length ℓ_c, as physically motivated earlier (eq. [12]).

Next, considering the limit of vanishing slab turbulence, we have $D_\perp = D_\perp^{\rm 2D}$, and

$$(D_\perp^{\rm 2D})^2 = \frac{1}{2\pi} \frac{1}{B_0^2} \int_{-\infty}^{\infty}\int_{-\infty}^{\infty} \frac{P_{xx}^{\rm 2D}(k_x, k_y)}{k_\perp^2} \times \left[1 - g(D_\perp k_\perp^2 \Delta z)\right] dk_x\, dk_y. \quad (33)$$

(A note on notation: $D_\perp^{\rm 2D}$ refers to the perpendicular random walk in the limit of no slab turbulence, while $\langle \Delta x^2 \rangle_{\rm 2D}$ refers to the contribution of two-dimensional turbulence even if slab turbulence is present.) Since g acts as a low-pass filter, $1 - g$ acts as a high-pass filter, which is close to 1 except that it becomes small within a "hole" in (k_x, k_y) space, for $k_\perp \lesssim |1/(D_\perp \Delta z)|^{1/2}$. As $\Delta z \to \infty$, the width of this hole decreases, and our expression for $D_\perp^{\rm 2D}$ is equivalent to that of Matthaeus et al. (1995). The effect of the hole around $k_\perp = 0$ is negligible if its size is much smaller than $k_{0\perp}$, so the expression

$$D_\perp^{\rm 2D} = \sqrt{\frac{1}{2\pi} \frac{1}{B_0^2} \int_{-\infty}^{\infty}\int_{-\infty}^{\infty} \frac{P_{xx}^{\rm 2D}(k_x, k_y)}{k_\perp^2} dk_x\, dk_y} \quad (34)$$

is valid for $k_{0\perp}^2 D_\perp \Delta z \gg 1$, i.e., $\langle \Delta x^2 \rangle \gg \ell_\perp$, for perpendicular excursions greater than the scale $\ell_\perp = 1/k_{0\perp}$. Referring to the flux function (vector potential) $a(x, y)$ for the two-dimensional turbulence (see § 2), we have

$$P_{xx}^{\rm 2D}(k_x, k_y) = k_y^2 A(k_\perp) \quad \text{and} \quad P_{yy}^{\rm 2D}(k_x, k_y) = k_x^2 A(k_\perp), \quad (35)$$

where $A(k_\perp)$, the (axisymmetric) power spectrum of $a(x, y)$, is defined as the Fourier transform of the correlation function $\langle a(0, 0) a(x, y) \rangle$. Then $P_{xx}^{\rm 2D} + P_{yy}^{\rm 2D} = k_\perp^2 A$, and assuming axisymmetry, the integral of $P_{xx}^{\rm 2D}/k_\perp^2$ is one-half that of A. Thus, we can relate $D_\perp^{\rm 2D}$ to the variance of $a(x, y)$:

$$D_\perp^{\rm 2D} = \sqrt{\frac{1}{2\pi} \frac{1}{2B_0^2} \int_{-\infty}^{\infty}\int_{-\infty}^{\infty} A(k_\perp)\, dk_x\, dk_y} = \sqrt{\frac{\langle a^2 \rangle}{2B_0^2}}, \quad (36)$$

and finally we can define the "ultrascale"

$$\tilde{\lambda} \equiv \sqrt{\frac{\langle a^2 \rangle}{\langle b^2 \rangle^{\rm 2D}}}, \quad (37)$$

again yielding a form that was physically motivated earlier (eq. [14]):

$$D_\perp^{\rm 2D} = \frac{\tilde{\lambda}}{\sqrt{2}} \frac{\sqrt{\langle b^2 \rangle^{\rm 2D}}}{B_0}. \quad (38)$$

By way of an analogy with hydrodynamic correlation functions (Batchelor 1953), we see that $\tilde{\lambda}$ is the length associated with the curvature of the $\langle aa' \rangle$ correlation at zero separation (see eq. [37]) and therefore may be thought of as the Taylor microscale, or "inner scale," of the $\langle aa' \rangle$ correlation function.

In summary, substituting equations (29) and (33) into equation (28) gives

$$D_\perp = D_\perp^{\rm slab} + \frac{(D_\perp^{\rm 2D})^2}{D_\perp},$$

$$D_\perp = \frac{D_\perp^{\rm slab}}{2} + \sqrt{\left(\frac{D_\perp^{\rm slab}}{2}\right)^2 + (D_\perp^{\rm 2D})^2}. \quad (39)$$

for $D_\perp^{\rm slab}$ and $D_\perp^{\rm 2D}$ as in equations (32) and (38), respectively (Matthaeus et al. 1995). We recall that this derivation assumes a diffusive random walk of the field line, which is valid only in the regime where $\langle \Delta x^2 \rangle \propto \Delta z$. This is true of the results for large Δz as given above, and evaluating $\langle \Delta x^2 \rangle$ on the basis of this formula for $D_\perp$ verifies that the range of validity is for $\langle \Delta x^2 \rangle^{1/2}$ and Δz greater than the respective coherence lengths. This built-in check of the range of validity arises from not approximating the limits of $d\Delta z'$ integration as $\pm\infty$. Equation (28) agrees with previous results while also providing a built-in

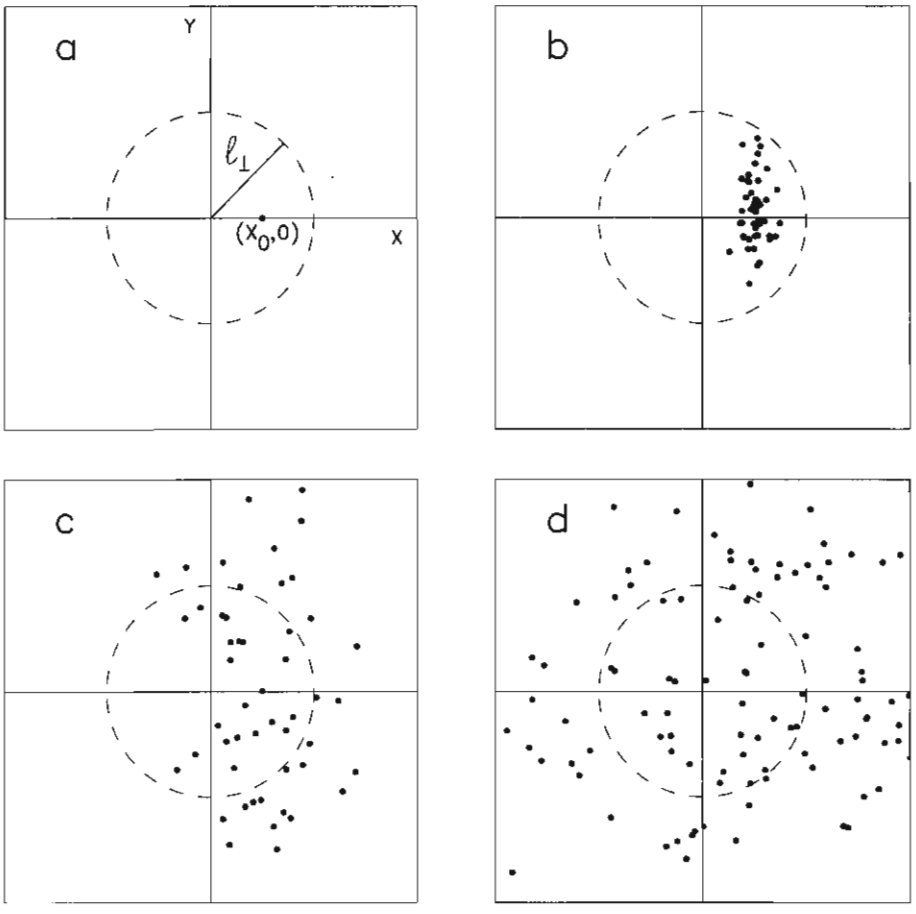

FIG. 4.—Schematic of the separation of field lines, i.e., the change in displacement (X, Y) between two field lines for a small initial displacement $(X_0, 0)$. (*a*) Two-dimensional turbulence is strongly correlated only for displacements within the dashed circle, of less than a perpendicular coherence length $\ell_\perp$. (*b–d*) Distribution of field line displacements with increasing Δz. (*b*) Slow diffusive separation. (*c*) Superdiffusive separation. (*d*) Fast diffusive separation.

check on the regime of validity. This is important in the following derivation of the field line separation.

4. SEPARATION OF TWO FIELD LINES

4.1. *Mathematical Derivation*

In this section, we derive the separation of two magnetic field lines in two-component 2D+slab turbulence. Now we consider the lateral coordinates of two different field lines, $x_1(z)$, $y_1(z)$, $x_2(z)$, and $y_2(z)$, expressing the displacement between them by $X \equiv x_1 - x_2$ and $Y \equiv y_1 - y_2$ (see Figs. 1 and 3). Without loss of generality, we consider $X(z = 0) = X_0$ and $Y(z = 0) = 0$; i.e., the x-direction is defined to be along the displacement between the two field lines at $z = 0$. Then the separation of the field lines is expressed as the change in displacement, $(\Delta X, \Delta Y)$, as a function of distance Δz along the mean magnetic field.

Note that although the turbulence can be assumed to be statistically homogeneous and axisymmetric in position space (x, y), the same cannot be said for displacement space (X, Y) (see Fig. 4). In particular, when one considers the correlation between the two-dimensional component of the turbulent field, $\boldsymbol{b}^{2D}$, at the positions of the two field lines, there is a fundamental difference between a distance much less than $\ell_\perp$ (strong correlation) and a distance much greater than $\ell_\perp$ (weak correlation). When we define the initial displacement as $(X_0, 0)$, then the separation in the two directions, ΔX and ΔY, need not be statistically identical, as we show mathematically in this section. Physically, ΔX initially represents a changing distance between the two field lines, while ΔY initially implies a changing orientation of the displacement (Fig. 4). After a large Δz, when $\langle \Delta X^2 \rangle^{1/2}$ and $\langle \Delta Y^2 \rangle^{1/2}$ are both much greater than $\ell_\perp$, the separation becomes axisymmetric, with $\langle \Delta X^2 \rangle^{1/2} \approx \langle \Delta Y^2 \rangle^{1/2}$.

Let us first treat ΔX, the x-separation between two field lines after a distance Δz, which can be expressed as (Jokipii 1973)

$$\Delta X = \Delta x_1 - \Delta x_2 = \frac{1}{B_0} \int_0^{\Delta z} \left[b_x(x_1', y_1', z') - b_x(x_2', y_2', z') \right] dz'. \tag{40}$$

Then we have

$$\begin{aligned} \langle \Delta X^2 \rangle = & \frac{1}{B_0^2} \int_0^{\Delta z} \int_0^{\Delta z} \langle b_x(x_1', y_1', z') b_x(x_1'', y_1'', z'') \rangle \, dz' \, dz'' \\ & + \frac{1}{B_0^2} \int_0^{\Delta z} \int_0^{\Delta z} \langle b_x(x_2', y_2', z') b_x(x_2'', y_2'', z'') \rangle \, dz' \, dz'' \\ & - \frac{1}{B_0^2} \int_0^{\Delta z} \int_0^{\Delta z} \langle b_x(x_1', y_1', z') b_x(x_2'', y_2'', z'') \rangle \, dz' \, dz'' \\ & - \frac{1}{B_0^2} \int_0^{\Delta z} \int_0^{\Delta z} \langle b_x(x_2', y_2', z') b_x(x_1'', y_1'', z'') \rangle \, dz' \, dz''. \end{aligned} \tag{41}$$

From the symmetry of "1" and "2" indices, we have

$$\langle \Delta X^2 \rangle = 2I_{11} - 2I_{12}, \tag{42}$$

where we define

$$I_{11} = \langle \Delta x^2 \rangle = \frac{1}{B_0^2} \int_0^{\Delta z} \int_0^{\Delta z} \langle b_x(x_1', y_1', z') b_x(x_1'', y_1'', z'') \rangle \, dz' \, dz'', \tag{43}$$

$$I_{12} = \frac{1}{B_0^2} \int_0^{\Delta z} \int_0^{\Delta z} \langle b_x(x_1', y_1', z') b_x(x_2'', y_2'', z'') \rangle \, dz' \, dz''. \tag{44}$$

Since slab fluctuations are independent of x- and y-coordinates, the contributions of slab turbulence to I_{11} and I_{12} are equal. Thus, the direct slab contributions to $\langle \Delta X^2 \rangle$ cancel, which makes sense because in pure slab turbulence the two field lines maintain a constant relative displacement at all z. This leaves us with

$$\langle \Delta X^2 \rangle = 2\langle \Delta x^2 \rangle_{2D} - \frac{2}{B_0^2} \int_0^{\Delta z} \int_0^{\Delta z} \langle b_x^{2D}(x_1', y_1', z') b_x^{2D}(x_2'', y_2'', z'') \rangle \, dz' \, dz''. \tag{45}$$

An equation for $\langle \Delta Y^2 \rangle$ can be obtained by the substitutions $\Delta X \to \Delta Y$, $\Delta x \to \Delta y$, and $b_x \to b_y$; with the assumption of axisymmetry in x and y, we have $\langle \Delta x^2 \rangle = \langle \Delta y^2 \rangle$. Note that although the direct slab contributions have cancelled, the presence of slab turbulence still affects the results in that both terms on the right-hand side of equation (45) implicitly involve the total perpendicular diffusion coefficient, $D_\perp = \langle \Delta x^2 \rangle / (2\Delta z)$ (including the slab contribution).

The calculation of the field line separation for a given Δz proceeds as in § 3. With the assumption of homogeneity, and again treating ΔX first,

$$\langle \Delta X^2 \rangle = 2\langle \Delta x^2 \rangle_{2D} - \frac{2}{B_0^2} \int_0^{\Delta z} \int_{-z'}^{\Delta z - z'} \langle b_x^{2D}(0,0,0) \times b_x^{2D}(\Delta x_2' - X', \Delta y_2' - Y', \Delta z') \rangle \, d\Delta z' \, dz'. \tag{46}$$

Suppressing "2" subscripts and using the simplified notation $X' \to X$, $Y' \to Y$, and $z' \to z$, we have

$$\langle \Delta X^2 \rangle = 2\langle \Delta x^2 \rangle_{2D} - \frac{2}{B_0^2} \int_0^{\Delta z} \int_{-z}^{\Delta z - z} \langle b_x^{2D}(0,0,0) b_x^{2D} \times (\Delta x' - X, \Delta y' - Y, \Delta z') \rangle \, d\Delta z' \, dz. \tag{47}$$

Here the displacement between x_2'' and x_1' is expressed in terms of displacements from a common point x_2' as shown in Figure 3. Then Corrsin's hypothesis and the assumption of independence of X and Y displacements allow us to write

$$\langle \Delta X^2 \rangle = 2\langle \Delta x^2 \rangle_{2D} - \frac{2}{B_0^2} \frac{1}{2\pi} \int_{-\infty}^{\infty} \int_{-\infty}^{\infty} P_{xx}^{2D}(k_x, k_y) \times \left\{ \int_0^{\Delta z} \left[\int_{-z}^{\Delta z - z} \left(\int_{-\infty}^{\infty} e^{-ik_x \Delta x'} P(\Delta x' | \Delta z') \, d\Delta x' \right) \times \left(\int_{-\infty}^{\infty} e^{-ik_y \Delta y'} P(\Delta y' | \Delta z') \, d\Delta y' \right) d\Delta z' \right] \times \left[\int_{-\infty}^{\infty} e^{ik_x X} P(X|z) \, dX \right] \times \left[\int_{-\infty}^{\infty} e^{ik_y Y} P(Y|z) \, dY \right] dz \right\} dk_x \, dk_y. \tag{48}$$

We can evaluate the three square-bracketed expressions in turn, making use of Gaussian and diffusive conditional probability distributions. In the first, the $\Delta x'$ and $\Delta y'$ integrals (inside parentheses) can be evaluated as in equation (24), after which the $\Delta z'$ integral is straightforward:

$$\int_{-z}^{\Delta z - z} \left(\int_{-\infty}^{\infty} e^{-ik_x \Delta x'} P(\Delta x' | \Delta z') \, d\Delta x' \right) \times \left(\int_{-\infty}^{\infty} e^{-ik_y \Delta y'} P(\Delta y' | \Delta z') \, d\Delta y' \right) d\Delta z' = \frac{1}{D_\perp k_\perp^2} \left(2 - e^{-D_\perp k_\perp^2 (\Delta z - z)} - e^{-D_\perp k_\perp^2 z} \right). \tag{49}$$

For the second bracketed expression, we note that $X = X_0 + \Delta X$, where X_0 is the initial displacement between the two field lines. Then

$$\int_{-\infty}^{\infty} e^{ik_x X} P(X|z) \, dX = e^{ik_x X_0} \int_{-\infty}^{\infty} e^{ik_x \Delta X} P(\Delta X | z) \, d\Delta X = e^{ik_x X_0} e^{-D_{sx} k_x^2 z}, \tag{50}$$

again making use of equation (24), where $D_{sx} \equiv \langle \Delta X^2 \rangle / (2\Delta z)$ is the diffusion coefficient for the x-separation of two magnetic field lines. The third bracketed expression is similar:

$$\int_{-\infty}^{\infty} e^{ik_y Y} P(Y|z) \, dY = e^{-D_{sy} k_y^2 z}. \tag{51}$$

We note that defining the initial displacement as $(X_0, 0)$ breaks the axisymmetry of ΔX and ΔY (see also Fig. 4), so D_{sx} and D_{sy} may be distinct.

Substituting equations (27), (35), and (49)–(51) into equation (48) and performing the z-integration, we obtain a complete expression for $\langle \Delta X^2 \rangle$:

$$\langle \Delta X^2 \rangle = \frac{8\Delta z^2}{\langle \Delta x^2 \rangle} \frac{1}{2\pi B_0^2} \int_{-\infty}^{\infty} \int_{-\infty}^{\infty} \frac{k_y^2 A(k_\perp)}{k_\perp^2} \left\{ 1 - g\frac{\langle \Delta x^2 \rangle k_\perp^2}{2} - e^{ik_x X_0} \left[g\left(\frac{\langle \Delta X^2 \rangle k_x^2}{2} + \frac{\langle \Delta Y^2 \rangle k_y^2}{2} \right) - \frac{1}{2} g^t \left(\frac{\langle \Delta X^2 \rangle k_x^2}{2} + \frac{\langle \Delta Y^2 \rangle k_y^2}{2}, \frac{\langle \Delta x^2 \rangle k_\perp^2}{2} \right) - \frac{1}{2} g\left(\frac{\langle \Delta X^2 \rangle k_x^2}{2} + \frac{\langle \Delta Y^2 \rangle k_y^2}{2} + \frac{\langle \Delta x^2 \rangle k_\perp^2}{2} \right) \right] \right\} dk_x \, dk_y. \tag{52}$$

TABLE 1

TYPES OF SEPARATION OF TWO MAGNETIC FIELD LINES IN TWO-COMPONENT TURBULENCE

Random Walk and Separation[a]	Distance Range	Type of Separation
$\ell_\perp^2 \ll \langle \Delta x^2 \rangle$ and $\langle \Delta X^2 \rangle$	Long Δz	Fast diffusive separation
$\langle \Delta X^2 \rangle \sim \ell_\perp^2 \ll \langle \Delta x^2 \rangle$	Intermediate Δz (only for $D_\perp^{2D} \ll D_\perp^{slab}$)	Superdiffusive
$\langle \Delta X^2 \rangle \ll \ell_\perp^2 \ll \langle \Delta x^2 \rangle$	Intermediate Δz (only for $D_\perp^{2D} \ll D_\perp^{slab}$)	Slow diffusive separation
$\langle \Delta x^2 \rangle$ and $\langle \Delta X^2 \rangle \lesssim \ell_\perp^2$	Short Δz	Nondiffusive[b]

[a] The quantity $\langle \Delta x^2 \rangle$ is the mean squared "random walk," the perpendicular displacement of a single magnetic field line relative to the mean field. The quantity $\langle \Delta X^2 \rangle$ is the mean squared separation between two magnetic field lines; see also Fig. 1.

[b] If $D_\perp^{2D} \ll D_\perp^{slab}$, nondiffusive behavior applies at a short distance $\Delta z \lesssim \ell_z$ regardless of the magnitudes of $\langle \Delta x^2 \rangle$ and $\langle \Delta X^2 \rangle$.

where $g'(u, v) \equiv (e^{-u} - e^{-v})/(v - u)$ is a two-dimensional low-pass filter that approaches 1 when and only when both $u \ll 1$ and $v \ll 1$. The analogous expression for $\langle \Delta Y^2 \rangle$ is

$$\langle \Delta Y^2 \rangle = \frac{8\Delta z^2}{\langle \Delta x^2 \rangle} \frac{1}{2\pi B_0^2} \int_{-\infty}^{\infty} \int_{-\infty}^{\infty} \frac{k_x^2 A(k_\perp)}{k_\perp^2} \left\{ 1 - g\left(\frac{\langle \Delta x^2 \rangle k_\perp^2}{2} \right) - e^{ik_z X_0} \left[g\left(\frac{\langle \Delta X^2 \rangle k_x^2}{2} + \frac{\langle \Delta Y^2 \rangle k_y^2}{2} \right) - \frac{1}{2} g'\left(\frac{\langle \Delta X^2 \rangle k_x^2}{2} + \frac{\langle \Delta Y^2 \rangle k_y^2}{2}, \frac{\langle \Delta x^2 \rangle k_\perp^2}{2} \right) - \frac{1}{2} g\left(\frac{\langle \Delta X^2 \rangle k_x^2}{2} + \frac{\langle \Delta Y^2 \rangle k_y^2}{2} + \frac{\langle \Delta x^2 \rangle k_\perp^2}{2} \right) \right] \right\} dk_x\, dk_y, \tag{53}$$

which differs from $\langle \Delta X^2 \rangle$ only in that $k_y^2 A(k_\perp)$ is replaced by $k_x^2 A(k_\perp)$.

In terms of diffusion coefficients, we have

$$D_{sx} = \frac{2}{D_\perp} \frac{1}{2\pi B_0^2} \int_{-\infty}^{\infty} \int_{-\infty}^{\infty} \frac{k_y^2 A(k_\perp)}{k_\perp^2} \left\{ 1 - g\left(D_\perp k_\perp^2 \Delta z \right) - e^{ik_z X_0} \left[g\left(D_{sx} k_x^2 \Delta z + D_{sy} k_y^2 \Delta z \right) - \frac{1}{2} g'\left(D_{sx} k_x^2 \Delta z + D_{sy} k_y^2 \Delta z, D_\perp k_\perp^2 \Delta z \right) - \frac{1}{2} g\left(D_{sx} k_x^2 \Delta z + D_{sy} k_y^2 \Delta z + D_\perp k_\perp^2 \Delta z \right) \right] \right\} dk_x\, dk_y, \tag{54}$$

and

$$D_{sy} = \frac{2}{D_\perp} \frac{1}{2\pi B_0^2} \int_{-\infty}^{\infty} \int_{-\infty}^{\infty} \frac{k_x^2 A(k_\perp)}{k_\perp^2} \left\{ 1 - g\left(D_\perp k_\perp^2 \Delta z \right) - e^{ik_z X_0} \left[g\left(D_{sx} k_x^2 \Delta z + D_{sy} k_y^2 \Delta z \right) - \frac{1}{2} g'\left(D_{sx} k_x^2 \Delta z + D_{sy} k_y^2 \Delta z, D_\perp k_\perp^2 \Delta z \right) - \frac{1}{2} g\left(D_{sx} k_x^2 \Delta z + D_{sy} k_y^2 \Delta z + D_\perp k_\perp^2 \Delta z \right) \right] \right\} dk_x\, dk_y. \tag{55}$$

4.2. *Interpretation: Regimes of Diffusive Separation*

Fortunately, the low-pass filters g and g' facilitate the interpretation of the general behavior of the mean squared separation between two magnetic field lines, described by $\langle \Delta X^2 \rangle$ and $\langle \Delta Y^2 \rangle$ as functions of distance along the mean field, Δz. The behavior of $\langle \Delta X^2 \rangle$ is summarized in Table 1; that of $\langle \Delta Y^2 \rangle$ is similar.

The interpretation presented in this section has been confirmed by numerical evaluation of equations (26), (27), (52), and (53) with the MATHEMATICA program (Wolfram Research, Inc.). Results for specific numerical examples are shown in Figures 5 and 6; see Appendix for details, including the turbulence parameters. Figure 5 shows $\langle \Delta x^2 \rangle$ and $\langle \Delta X^2 \rangle$ as a function of Δz, with a log-log scale, so diffusive behavior corresponds to lines of slope 1, with a diffusion coefficient proportional to the intercept at $\log \Delta z = 0$. Regimes of diffusive behavior are highlighted with solid lines. Figure 6 shows diffusion coefficients D_{sx} and D_{sy} as functions of Δz, so here diffusive behavior corresponds to the flat portions of the curves. We must point out that the assumptions underlying our quantitative derivation are invalid if the behavior is nondiffusive. However, we can draw the qualitative conclusion that superdiffusive behavior "connects" the two diffusive regimes in Figures 5*b* and 6.

The regimes of behavior of the mean squared separation are controlled by the low-pass filters g and g'. The arguments of g and g' depend on quantities such as $\langle \Delta x^2 \rangle k_\perp^2$ or $\langle \Delta X^2 \rangle k_x^2$, and the k_x and k_y integrals are dominated by the region with $k_\perp \lesssim k_{0\perp}$, so the different regimes of behavior are defined by whether $\langle \Delta x^2 \rangle$ and $\langle \Delta X^2 \rangle$ are greater or less than the perpendicular coherence length squared, $\ell_\perp^2 = 1/k_{0\perp}^2$.

First, we consider the case where $\langle \Delta x^2 \rangle \gg \ell_\perp^2$ and $\langle \Delta X^2 \rangle \gg \ell_\perp^2$, which occurs at long distances Δz. In this case, all the g'- and g-terms tend to zero, and we have

$$\langle \Delta X^2 \rangle = \langle \Delta Y^2 \rangle = 2 \langle \Delta x^2 \rangle_{2D},$$
$$D_{sx} = D_{sy} = 2 \frac{(D_\perp^{2D})^2}{D_\perp} = \frac{1}{D_\perp} \frac{\langle a^2 \rangle}{B_0^2} = \frac{\tilde{\lambda}^2}{D_\perp} \frac{\langle b^2 \rangle^{2D}}{B_0^2}. \tag{56}$$

We see that in the long-distance limit, the field line separation is axisymmetric, independent of the starting displacement X_0, and diffusive with a diffusion coefficient twice as great as the two-dimensional contribution to the random walk. This behavior, which we refer to as fast diffusive separation, can be seen in the long-distance regimes of Figures 5 and 6. Note that for the case of a slab-dominated random walk ($D_\perp^{slab} \gg D_\perp^{2D}$),

$$D_{sx} = D_{sy} \approx \frac{2\tilde{\lambda}^2}{\ell_c} \frac{\langle b^2 \rangle^{2D}}{\langle b^2 \rangle^{slab}}, \tag{57}$$

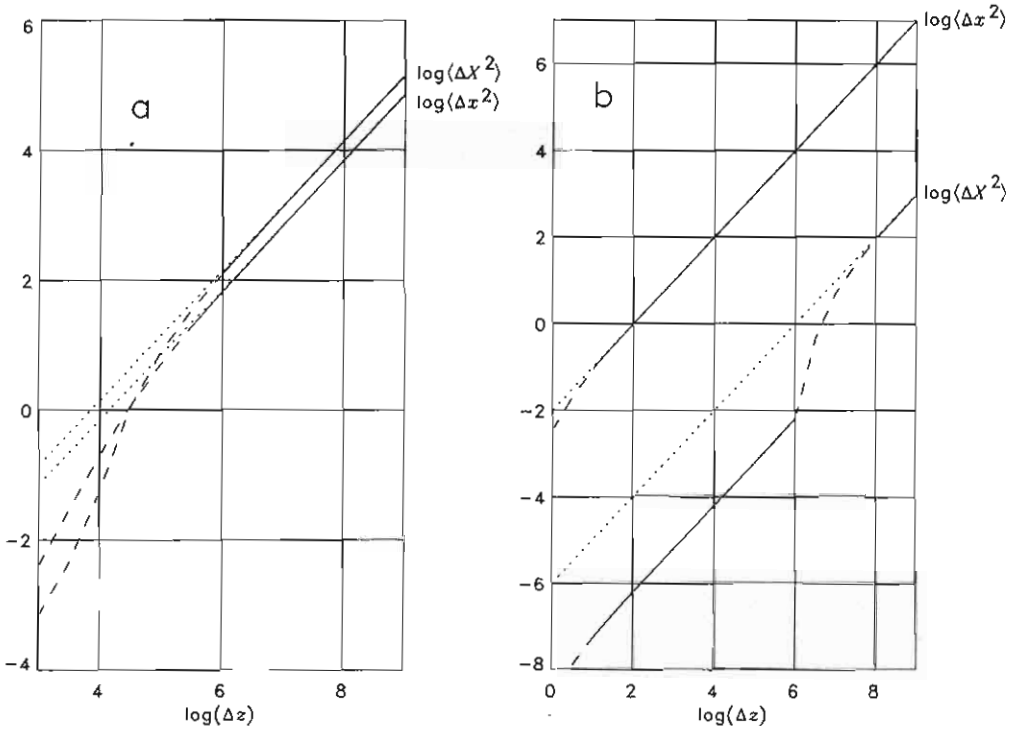

FIG. 5.—Examples of the field line random walk $\langle \Delta x^2 \rangle$ and separation $\langle \Delta X^2 \rangle$ as a function of Δz, the distance along the mean magnetic field. The random walk is dominated by (*a*) the two-dimensional component of turbulence, (*b*) the slab component of turbulence. Solid lines indicate diffusive behavior; dashed lines indicate superdiffusion. Dotted lines, for reference, show the extension of the long-distance behavior. Ordinates in units of $\ell_\perp^2$, abscissae in units of ℓ_c. (See text for details.)

and for a two-dimensional–dominated random walk we have

$$D_{sx} \simeq D_{sy} \approx \tilde{\lambda} \frac{\sqrt{2\langle b^2 \rangle^{2D}}}{B_0}. \tag{58}$$

To understand these results for fast diffusive separation, recall from § 1 that if two turbulent field lines were completely uncorrelated, undergoing independent random walks, the mean squared separation $\langle \Delta X^2 \rangle$ would be twice the mean squared random walk $\langle \Delta x^2 \rangle$ of one field line. In the 2D+slab model of turbulence, only the two-dimensional component decorrelates in the perpendicular directions, so we can understand why the fast diffusive separation in the long-distance limit is twice as great as the two-dimensional contribution to the random walk. Since this regime involves large separations and decorrelation of the two-dimensional turbulence at the two field lines, as shown in Figure 4*d*, we can also understand why this behavior is axisymmetric (with $\langle \Delta X^2 \rangle = \langle \Delta Y^2 \rangle$) and independent of the initial displacement between the field lines, X_0.

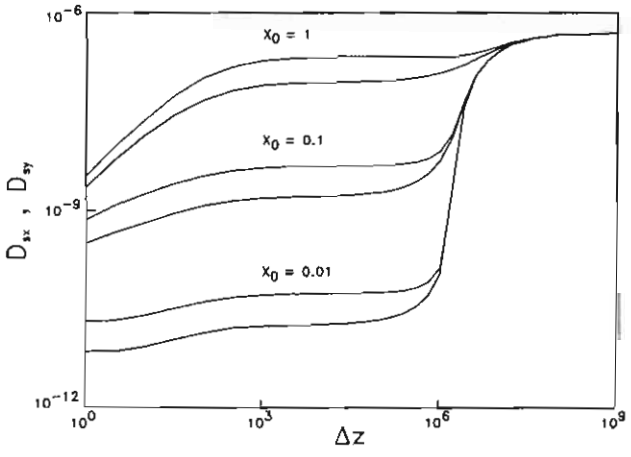

FIG. 6.—Coefficients of diffusive separation, D_{sx} (*thick lines*) and D_{sy} (*thin lines*), as a function of Δz for the slab-dominated case of Fig. 5*b* and various initial displacements X_0, with x-quantities in units of $\ell_\perp$ and z-quantities in units of ℓ_c.

Paradoxically, equation (56) implies that when the slab turbulent energy $\langle b^2 \rangle^{\rm slab}$ is increased, $D_\perp$ increases and the coefficient of diffusive separation *decreases* (as does the two-dimensional contribution to $D_\perp$; see eq. [39]). This is illustrated by Figures 5*a* and 5*b*, which differ only in the amplitude of slab turbulence (see the Appendix for details). An interpretation of this effect is that rapid lateral excursions due to slab turbulence quickly decorrelate the "random flights" in the relative excursions of the two field lines, ΔX and ΔY. The random flights depend on two-dimensional turbulence and hence x and y, which change more rapidly with increased slab turbulence. This yields a shorter mean free z-distance in the motion of one field line relative to another, hence the lower coefficient of diffusive separation.

Now let us consider what happens as Δz decreases. In the long-distance limit, we have fast diffusive separation where $\langle \Delta X^2 \rangle = 2\langle \Delta x^2 \rangle_{2D}$. In the case in which the two-dimensional component dominates the random walk, $D_\perp^{2D} \gtrsim D_\perp^{\rm slab}$, we indeed have $\langle \Delta X^2 \rangle \approx 2\langle \Delta x^2 \rangle$. That implies that these two quantities both reach $\ell_\perp^2$ at about the same distance Δz (Fig. 5*a*). When $\langle \Delta x^2 \rangle \lesssim \ell_\perp^2$ and $\langle \Delta X^2 \rangle \lesssim \ell_\perp^2$, then the low-pass filters g and g' switch on, our expressions for $\langle \Delta x^2 \rangle_{2D}$ and $\langle \Delta X^2 \rangle$ instead vary

as $(\Delta z)^2$, and our derivation is no longer valid in this regime. This indeed happens at short distances Δz even if the two-dimensional component does not dominate the random walk. Physically, we expect such behavior in the "free-streaming" limit where $\boldsymbol{b}$ is nearly unchanged in direction. Such non-diffusive behavior, the last case listed in Table 1, can be seen at low Δz in Figures 5 and 6.

Therefore, when the two-dimensional component dominates the random walk, the two quantities $\langle \Delta X^2 \rangle$ and $\langle \Delta x^2 \rangle$ are of the same order of magnitude. On the other hand, if the slab component dominates the random walk, we can have the field line random walk much greater than the field line separation because the slab fluctuations directly contribute to the former but not the latter. Furthermore, it is possible to have

$$\langle \Delta X^2 \rangle \ll \ell_\perp^2 \ll \langle \Delta x^2 \rangle, \tag{59}$$

which is intermediate to the short-distance and long-distance regimes described above. In this case, two nearby field lines follow highly correlated trajectories with a mutual separation much lower than the displacement from the mean field, as represented by the lower two field lines in Figure 1. We refer to this behavior as "slow diffusive separation."

Referring to equations (52)–(55) and recalling that the integrals are dominated by $k_\perp \lesssim k_{0\parallel} = 1/\ell_\perp$, we have $g' \to 0$ and $g \to 0$, with the exception that $g(\langle \Delta X^2 \rangle k_\perp^2/2) \to 1$, so

$$D_{sx} = \frac{2}{D_\parallel} \frac{1}{2\pi B_0^2} \int_{-\infty}^{\infty} \int_{-\infty}^{\infty} \frac{k_y^2 A(k_\perp)}{k_\parallel^2} \left(1 - e^{ik_x X_0}\right) dk_x\, dk_y, \tag{60}$$

$$D_{sy} = \frac{2}{D_\perp} \frac{1}{2\pi B_0^2} \int_{-\infty}^{\infty} \int_{-\infty}^{\infty} \frac{k_x^2 A(k_\perp)}{k_\perp^2} \left(1 - e^{ik_x X_0}\right) dk_x\, dk_y. \tag{61}$$

Recall that A is the power spectrum of $a(x, y)$, i.e., the Fourier transform of the autocorrelation function $\langle a(0,0)a(x,y) \rangle$. Thus, the directionally averaged coefficient of slow diffusive separation is

$$D_s \equiv \frac{D_{sx} + D_{sy}}{2} = \frac{1}{D_\perp} \frac{\langle a^2 \rangle - \langle a(0,0)a(X_0,0) \rangle}{B_0^2}. \tag{62}$$

This expression for D_s varies linearly with the autocorrelation of the flux function a at the initial displacement between the field lines and has a direct physical interpretation. If the field lines are initially far apart with $X_0 \gg \ell_\perp$, so that the correlation $\langle a(0,0)a(X_0,0) \rangle \to 0$, then we recover the expression for fast diffusive separation (eq. [56]). Physically, this refers to the separation between two field lines for uncorrelated two-dimensional turbulence (and perfectly correlated slab turbulence, at the same z-coordinate), and there is no difference from the fast diffusive separation regime. On the other hand, for $X_0 \lesssim \ell_\perp$, field lines are initially close together with a substantial correlation in the flux function a, and the coefficient of diffusive separation is slower in this regime.

Transforming equation (62) to obtain

$$D_s = \frac{1}{D_\perp} \frac{\langle [a(X_0,0) - a(0,0)]^2 \rangle}{2B_0^2}. \tag{63}$$

we see that this expression is also related to the mean squared difference between a at the positions of the two field lines. Note that $a(X_0, 0) - a(0, 0)$ can be interpreted as $\int_1^2 \boldsymbol{b}^{2D} \cdot \hat{\boldsymbol{n}}\, d\ell$, where $d\ell$ is the line element along any curve connecting the locations of field lines 1 and 2 and $\hat{\boldsymbol{n}}$ is the two-dimensional normal to that curve, i.e., the two-dimensional magnetic flux threading any such curve. There is an interesting similarity between this expression and equation (56) for fast diffusive separation.

Another property of slow diffusive separation is that it is nonaxisymmetric, i.e., $\langle \Delta Y^2 \rangle > \langle \Delta X^2 \rangle$. Recalling that the axisymmetry is broken by defining the initial displacement as $(X_0, 0)$, ΔX initially refers to the change in the distance between the two field lines, while ΔY implies a changing orientation of the displacement (Fig. 4). Mathematically, in the limit of small X_0 and with a transformation to polar coordinates $(k_\perp, \varphi)$, equations (60) and (61) become

$$D_{sx} = \frac{1}{D_\perp} \frac{X_0^2}{2\pi B_0^2} \left[\int_0^{2\pi} \sin^2\varphi \cos^2\varphi\, d\varphi \right] \int_0^{\infty} k_\perp^3 A(k_\perp)\, dk_\perp,$$

$$D_{sy} = \frac{1}{D_\perp} \frac{X_0^2}{2\pi B_0^2} \left[\int_0^{2\pi} \cos^4\varphi\, d\varphi \right] \int_0^{\infty} k_\perp^3 A(k_\perp)\, dk_\perp. \tag{64}$$

The bracketed integrals are $\frac{1}{4}\pi$ and $\frac{3}{4}\pi$, respectively, so for small X_0 the ratio of $\langle \Delta Y^2 \rangle$ to $\langle \Delta X^2 \rangle$ is 3:1. Using the relation $k_\perp^2 A = P_{xx}^{2D} + P_{yy}^{2D}$, we have

$$D_{sx} = \frac{1}{8} \frac{1}{D_\perp} \frac{\langle b^2 \rangle^{2D}}{B_0^2} X_0^2,$$

$$D_{sy} = \frac{3}{8} \frac{1}{D_\perp} \frac{\langle b^2 \rangle^{2D}}{B_0^2} X_0^2, \tag{65}$$

or in terms of the correlation of a, we have

$$D_{sx} = \frac{1}{2} \frac{1}{D_\perp} \frac{\langle a^2 \rangle - \langle a(0,0)a(X_0,0) \rangle}{B_0^2},$$

$$D_{sy} = \frac{3}{2} \frac{1}{D_\perp} \frac{\langle a^2 \rangle - \langle a(0,0)a(X_0,0) \rangle}{B_0^2}. \tag{66}$$

Note that when $\langle a^2 \rangle - \langle a(0,0)a(X_0,0) \rangle$ is expanded in terms of X_0, odd terms vanish by symmetry and the leading term is of order X_0^2. Numerical values of D_{sx} and D_{sy} are shown in Figure 6 for various values of X_0 (in units of $\ell_\perp$).

Figure 4 also illustrates the transition between slow diffusive separation and fast diffusive separation for a slab-dominated random walk and for $X_0 \lesssim \ell_\perp$. When the two field lines are closer than $\ell_\perp$, the two-dimensional fluctuations are strongly correlated, leading to slow diffusive separation. The distribution of the field line separation is nonaxisymmetric, preferentially changing the direction of the displacement instead of the distance. This is related to the motion of field lines subject to two-dimensional turbulence: at any given position, two field lines are typically both rotating around the same two-dimensional "island." The mutual random walk is suppressed by the temporary confinement of field lines within a perpendicular coherence length. When the distance is of order $\ell_\perp$, the two-dimensional fluctuations decorrelate and the rate of separation increases. This is a regime of superdiffusion that bridges between the slow diffusive separation and fast diffusive separation (also seen in Figs. 5 and 6). Then for distances much greater than $\ell_\parallel$ one obtains the long-distance limit of fast diffusive separation, which is axisymmetric and independent of X_0. The various regimes of field line separation of summarized in Table 1.

In Figure 6, it is seen that the onset of superdiffusive behavior occurs at a certain Δz value, independent of X_0. This is similar to the behavior of the mean separation versus z in Figure 2 of Maron et al. (2004). This can be understood in terms of a universal curve of $\langle R^2 \rangle$ versus z, defined by the *Ansatz*

$$\frac{d\langle R^2 \rangle}{dz} = 4D_s(\langle R^2 \rangle). \tag{67}$$

Here the function $D_s(\langle R^2 \rangle)$ is a running diffusion coefficient, related but not necessarily identical to the diffusion coefficient derived earlier, and $\langle R^2 \rangle$ refers to the mean squared distance between the two field lines,

$$\langle R^2 \rangle \equiv \langle X^2 \rangle + \langle Y^2 \rangle = X_0^2 + \langle \Delta X^2 \rangle + \langle \Delta Y^2 \rangle. \tag{68}$$

The value of $D_s(\langle R^2 \rangle)$ is set to $D_s(X_0^2)$ from the slow diffusive separation regime (in which $\langle \Delta X^2 + \Delta Y^2 \rangle \ll X_0^2$ and $\langle R^2 \rangle \approx X_0^2$) as given by equation (62). The above *Ansatz* proposes that D_s is a function only of $\langle R^2 \rangle$ and not a function of the details of the displacement distribution, which is particularly accurate for slow diffusive separation and the onset of superdiffusion (e.g., eq. [65] shows that $D_s \propto X_0^2$, so replacing X_0^2 by the mean $\langle R^2 \rangle$ leaves D_s nearly unchanged). Then the choice of X_0 is viewed as the choice of a starting point $(z_0, \langle R^2 \rangle = X_0^2)$ along the universal curve, with $\langle \Delta X^2 + \Delta Y^2 \rangle = \langle R^2 \rangle - X_0^2$ and $\Delta z = z - z_0$. This model can approximately reproduce the results in Figure 6 for slow diffusive separation and the onset of superdiffusion. In that range, using $D_\perp \approx D_\perp^{\rm slab}$ and from equations (32) and (65), we have

$$D_s(\langle R^2 \rangle) = \frac{\langle b^2 \rangle^{\rm 2D}}{\langle b^2 \rangle^{\rm slab}} \frac{\langle R^2 \rangle}{2\ell_c}, \tag{69}$$

and solving equation (67) we obtain

$$\langle R^2 \rangle = X_0^2 e^{\Delta z/\ell_g},$$
$$\langle \Delta X^2 + \Delta Y^2 \rangle = X_0^2 \left(e^{\Delta z/\ell_g} - 1 \right), \tag{70}$$

where the exponential growth length along the mean magnetic field,

$$\ell_g = \frac{\ell_c}{2} \frac{\langle b^2 \rangle^{\rm slab}}{\langle b^2 \rangle^{\rm 2D}}, \tag{71}$$

marks the end of the approximately linear dependence of $\langle \Delta X^2 + \Delta Y^2 \rangle$ on Δz, i.e., the end of slow diffusive separation. In this way, the onset of superdiffusion can be viewed as part of a process of exponential growth of $\langle R^2 \rangle$ as a function of z, which is an example of stochastic instability. The result (eq. [71]) amounts to a calculation of the Kolmogorov-Lyapunov length (Rechester & Rosenbluth 1978) for a slab-dominated two-component magnetic field turbulence mode.

5. COMPUTER SIMULATIONS

To confirm the conclusions of these analytic calculations, we also developed computer simulations of field line separation in 2D+slab turbulence. While the simulations inevitably involve some discretization and statistical errors, they do avoid the key assumptions of the analytic work (Corrsin's hypothesis, Gaussian probability distributions, and diffusive separation) and thus provide an independent check of their validity. Computer simulations are also useful for examining the regimes in which our analytic expressions are not valid, i.e., where the field line separation is not diffusive. The basic methods and results are presented here, and more technical details can be found in the Appendix.

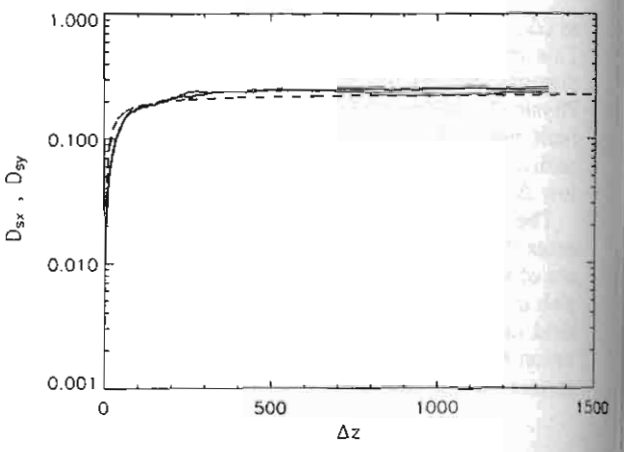

FIG. 7.—Coefficients of diffusive separation derived from computer simulations, D_{sx} (*thick solid line*) and D_{sy} (*thin solid line*), compared with $D_{sx} = D_{sy}$ from analytic calculations (*dashed line*), as a function of Δz for a random walk dominated by the two-dimensional component of turbulence. The long-distance limit is the regime of fast diffusive separation. (See text for details.)

The simulations involved two steps:

1. Generating representations of slab and two-dimensional turbulence with desired statistical properties, such as a power spectrum that follows the Kolmogorov power law over the inertial wavenumber range and rolls over in the energy-containing range, as observed for solar wind turbulence (Jokipii & Coleman 1968). (See the Appendix for mathematical expressions.) Random phases are used in wavenumber space, followed by inverse fast Fourier transforms to obtain $\boldsymbol{b}^{\rm slab}(z)$ and $\boldsymbol{b}^{\rm 2D}(x, y)$. The transforms in z used 2^{23} ($\approx 8.4 \times 10^6$) points, while the transforms in x and y used $2^{12} = 4096$ points in each dimension.

2. Tracing magnetic field lines, i.e., solving the coupled ordinary differential equations

$$\frac{dx}{dz} = \frac{b_x(x, y, z)}{B_0}, \quad \frac{dy}{dz} = \frac{b_y(x, y, z)}{B_0}. \tag{72}$$

We used a fourth-order Runge-Kutta method with adaptive time stepping regulated by a fifth-order error estimate step (Press et al. 1992). The D_{sx} and D_{sy} values were based on averages over 1000 pairs of field lines, and each pair was for a distinct realization of slab and two-dimensional turbulence.

Now the key physical conclusions of the analytic work (Table 1) can be checked using the computer simulations. In the two-dimensional–dominated case, where $D_\perp^{\rm 2D} \gtrsim D_\perp^{\rm slab}$, we expect a nondiffusive (free-streaming) regime at short Δz, followed by fast diffusive separation at long Δz (where $\langle \Delta x^2 \rangle \gtrsim \ell_\perp^2$). The analytic expression is expected to hold quantitatively for diffusive behavior in the long-distance limit; in particular, the fast diffusive separation rate should be given by equation (56).

Figure 7 shows a specific example of two-dimensional-dominated behavior. Specifically, we used $\langle b^2 \rangle^{\rm 2D} = \langle b^2 \rangle^{\rm slab} = B_0^2/8$, $X_0 = 0.1339$, and other parameters as in the Appendix.

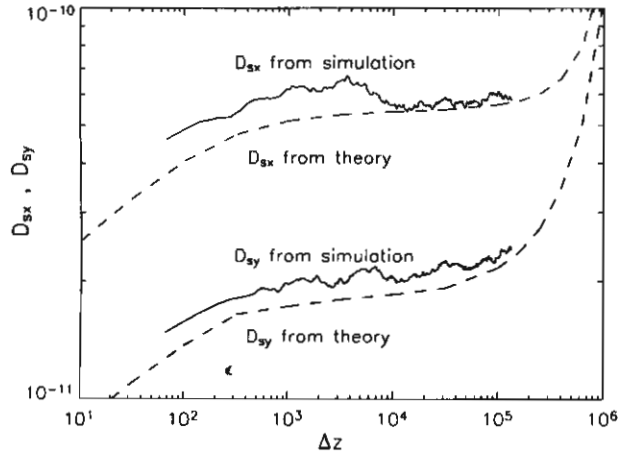

FIG. 8.—Coefficients of diffusive separation derived from computer simulations, D_{ss} (*thick solid line*) and D_{sy} (*thin solid line*), compared with those from analytic calculations (*thick dashed line and thin dashed line, respectively*), as a function of Δz for a random walk dominated by the slab component of turbulence, in the regime of slow diffusive separation. (See text for details.)

These yield $D_{\perp}^{2D} = 0.144$ and $D_{\perp}^{slab} = 0.0625$. The computational box sizes were $L_z = 10^6 \ell_z$ and $L_x = L_y = 200\ell_z$. The simulation results for D_{sx} (*thick solid line*) and D_{sy} (*thin solid line*) are compared with the analytic predictions for D_{sx} and D_{sy} from equations (54) and (55), which are indistinguishable in Figure 7 (*dashed line*). The difference of about 10% at large Δz represents good quantitative agreement, given the simulation uncertainties. These include the statistical uncertainty, as estimated from the difference between simulation results for D_{sx} and D_{sy} and their stochastic variation with Δz, and the discretization error of about 6%, which we estimate by replacing continuous integration over $\boldsymbol{k}$ in the analytic expressions with discrete sums over the $\boldsymbol{k}$-modes used in the simulations. Note also that the analytic expression correctly identifies the Δz range in which diffusive separation behavior begins, i.e., the lower limit of applicability of the diffusion approximation.

Another simulation with the same total turbulent energy but a 20:80 ratio of $\langle b^2 \rangle^{slab}$ to $\langle b^2 \rangle^{2D}$ showed a similar level of agreement. Indeed, agreement on the order of 15% was also found between computer simulations and analytic calculations for the field line random walk (Gray et al. 1996). In addition to the long-distance limit, another noteworthy feature of our two-dimensional–dominated simulations is that in the free-streaming regime, there is nonaxisymmetric separation, $D_{sy} > D_{sx}$, reminiscent of the analytic results in the slow diffusive regime for the slab-dominated case (see also Fig. 4).

The interesting features of analytic results for the slab-dominated case ($D_{\perp}^{slab} \gg D_{\perp}^{2D}$) are a regime of nonaxisymmetric slow diffusive separation, with $D_{sy} \approx 3D_{sx}$, followed by a superdiffusive transition to fast diffusive separation in the long-distance limit. We performed computer simulations for the same parameter values as in Figures 5*b* and 6, with the exception that X_0 was set to 0.01. The computational box sizes were $L_z = 2 \times 10^6 \ell_z$ and $L_x = L_y = 200\ell_z$. The comparison with analytic calculations (Fig. 8) demonstrates good agreement, with both simulation and analytic values flattening over the same range of Δz at the ratio $D_{sy}/D_{sx} \approx 3$. The difference of ~15% is again of the same order as the statistical and discretization errors in the simulations (the latter is estimated at 10%–15%) and is similar to that obtained by Gray et al. (1996).

Note that in the slab-dominated case, the slow diffusion and onset of superdiffusion can also be expressed as an exponential separation phase (see § 4.2). When fitting the computational results for $\langle R^2 \rangle = X_0^2 + \langle \Delta X^2 \rangle + \langle \Delta Y^2 \rangle$ to an exponential function of z, we find that the best fit is for $\langle R^2 \rangle = 9.97 \times 10^{-5} \exp(-z/6.57 \times 10^5)$. Referring to equations (70) and (71), the analytic expectation is $\langle R^2 \rangle = X_0^2 \exp(-z/\ell_g)$, where for this case $X_0^2 = 10^{-4}$ and $\ell_g = 6.67 \times 10^5$. Thus, the analytic and numerical calculations agree to within 0.3% for the prefactor and to within 1.5% for the exponential growth length, ℓ_g.

6. DISCUSSION AND CONCLUSIONS

We have developed an analytic formalism for the ensemble-averaged field line random walk and separation that does not assume a long-distance limit, i.e., in which fluctuations between the two field lines have not completely decorrelated. This is possible by retaining finite limits of integration in $\Delta z'$. The results of the analytic theory have been confirmed by numerical simulations, justifying the use of Corrsin's hypothesis.

The analytic results we have derived are nonperturbative in the sense that neither the total turbulent energy nor the turbulent energy of the slab or the two-dimensional component is constrained to be small. The results are also not restricted to a specific functional form for the power spectrum. We consider a particular case of anisotropic turbulence, in which power in $\boldsymbol{k}$-space is concentrated along the parallel axis and (axisymmetrically) along the perpendicular plane.

With its idealized and clear separation of parallel and perpendicular fluctuations, the two-component magnetic turbulence model considered here is an archetype of highly anisotropic turbulence, which also serves as a useful model of turbulence in the solar wind (Matthaeus et al. 1990; Bieber et al. 1996) and has helped to quantitatively explain solar energetic particle transport (Bieber et al. 1994). In comparison, in the work of Jokipii (1973) all the turbulence is taken to decorrelate after a certain z-distance. In this sense it is like the slab component in our work but differs in that it also contributes to field line separation. The results of Jokipii (1973) were generalized by Zimbardo et al. (1984) to other mean field geometries.

Our overall picture of diffusive separation at long distances and nondiffusive separation at short distances, with possible regimes of slow diffusion and superdiffusion in between, is qualitatively consistent with that presented by Isichenko (1991a, 1991b) for general magnetic turbulence. As discussed in the previous section, the slow diffusion and onset of superdiffusion in the mean squared separation $\langle \Delta X^2 + \Delta Y^2 \rangle$ can be identified as an exponential growth of the mean squared distance between two field lines, $\langle R^2 \rangle$, as discussed by various authors (e.g., Skilling et al. 1974; Rechester & Rosenbluth 1978; Krommes 1978; Similon & Sudan 1989; Isichenko 1991a, 1991b and references therein). It was shown by Barghouty & Jokipii (1996) that the results of Jokipii (1973) can also be interpreted in such terms. In terms of the separation of field lines, we have shown that there is a regime that can be usefully considered as diffusive and nonaxisymmetric in the perpendicular directions (slow diffusive separation; Figs. 4, 5, 6, and 8).

In our detailed work for the particular case of two-component turbulence, we find a criterion for different types of field line

separation behavior that is somewhat different from that of Isichenko (1991a, 1991b). That work, as well as Krommes (1978) and Kadomtsev & Pogutse (1979), stressed a parameter R given (in our notation) by

$$R \sim \frac{\sqrt{\langle b^2 \rangle}}{B_0} \frac{\ell_z}{\ell_\perp}, \tag{73}$$

sometimes called the Kubo number. On the other hand, our work identifies regimes of behavior that depend on $D_\perp^{\rm slab}/D_\perp^{\rm 2D}$, the ratio of contributions to the field line random walk, which are in turn related to the amplitude of each component and the relevant distance scales. (Recall that $D_\perp^{\rm 2D}$ contains $\tilde{\lambda}$, the ultrascale, which is in general distinct from the perpendicular coherence scale $\ell_\perp$.) Both $D_\perp$ and D_s have different dependences for $D_\perp^{\rm slab}/D_\perp^{\rm 2D} \gg 1$ or $\ll 1$ (compare eqs. [32] and [38] with eqs. [57] and [58]).

Can we reconcile the role of R in previous studies with the role of $D_\perp^{\rm slab}/D_\perp^{\rm 2D}$ in our work? We note that the previous work that considered R as a key parameter did not specifically consider turbulence with very different amplitudes for quasi-parallel and quasi-perpendicular wavevectors $\boldsymbol{k}$, apparently making the implicit assumption that those amplitudes are comparable. Indeed, the ratio

$$\frac{D_\perp^{\rm slab}}{D_\perp^{\rm 2D}} = \frac{\langle b^2 \rangle^{\rm slab}/B_0^2}{\sqrt{\langle b^2 \rangle^{\rm 2D}}/B_0} \frac{\ell_c/2}{\tilde{\lambda}/\sqrt{2}} \tag{74}$$

reduces to R (modulo constants of order unity) in the case where $\langle b^2 \rangle^{\rm slab} \sim \langle b^2 \rangle^{\rm 2D}$ and $\tilde{\lambda} \sim \ell_\perp$. Therefore, we suggest that the ratio of contributions to $D_\perp$ from quasi-parallel and quasi-perpendicular wavevectors $\boldsymbol{k}$ may be a more general criterion for determining the behavior of field line separation in anisotropic turbulence.

The exponential growth rate for the mean squared distance, which has also been called the Kolmogorov entropy or topological entropy (see Appendix B of Isichenko 1991b), is also found to be different for various cases of magnetic turbulence (Jokipii 1973; Barge et al. 1984; Similon & Sudan 1989; Isichenko 1991a, 1991b; Barghouty & Jokipii 1996; Maron et al. 2004), showing that general expressions are not always applicable to particular cases of interest. In our case of two-component turbulence, the exponential growth length, given by equation (71), is again related to the ratio between the amplitudes of slab and two-dimensional components of the turbulent magnetic field, not only correlation lengths and the overall amplitude as suggested by Isichenko (1991a, 1991b).

Now let us return to a specific issue raised in § 1: can observed dropouts (i.e., sharp spatial gradients) of solar energetic particles be explained by field line separation in the solar wind that is much slower than the field line random walk? Apparently not, because observed particle motion and magnetic turbulence in the solar wind are best modeled by a roughly 80 : 20 ratio in two-dimensional : slab turbulent energy (Bieber et al. 1994, 1996), and $\tilde{\lambda}$ is inferred from observations to be $\sim$0.2 AU (Matthaeus et al. 1999), so the derived value of $D_\perp^{\rm 2D} = 0.37$ AU is about an order of magnitude higher than the slab contribution. This corresponds to a two-dimensional-dominated random walk, the case of Figure 5*a*, and we expect fast diffusive separation ($D_s \approx 2D_\perp^{\rm 2D}$) for distances greater than a parallel coherence length of $\sim$0.02 AU. Therefore, field line separation should correspond to uncorrelated random walks of two field lines starting in the same region. An alternative explanation of dropouts, corresponding to temporary trapping of field lines near O-points in the turbulence, is presented by Ruffolo et al. (2003).

In conclusion, we use nonperturbative analytic techniques based on the Corrsin independence hypothesis and computer simulations to investigate the separation of magnetic field lines in a two-component model of anisotropic turbulence, which has proven to be a useful model of turbulence in the solar wind. In the long-distance limit, we predict "fast diffusive separation" with a diffusion coefficient $D_s \approx 2(D_\perp^{\rm 2D})^2/D_\perp$, where $D_\perp$ refers to the perpendicular diffusion (random walk) of field lines relative to the (constant) mean magnetic field and $D_\perp^{\rm 2D}$ is for the case of vanishing slab turbulence. This has the counterintuitive implication that increasing slab turbulence leads to a smaller D_s. If the random walk is dominated by the two-dimensional component of turbulence, fast diffusive separation begins as soon as the random walk reaches a perpendicular coherence length $\ell_\perp$. However, if the slab component dominates the random walk, there is more interesting behavior at intermediate Δz. We find nonaxisymmetric, slow diffusive separation at a rate related to the correlation of the flux function (vector potential) at the initial separation, followed by super-diffusive separation at $\Delta z \gtrsim \ell_g$, which increases up to the fast diffusive separation rate. The length ℓ_g is identified with an exponential growth scale for the distance between neighboring magnetic field lines, which is related to the relative amplitudes of the slab and two-dimensional components.

D. R. greatly appreciates the hospitality of the Bartol Research Institute, University of Delaware, where this work was conceived. This research was partially supported by a Basic Research Grant and a Royal Golden Jubilee Fellowship from the Thailand Research Fund, the Rachadapisek Sompoj Fund of Chulalongkorn University, and the NASA Sun-Earth Connections Theory Program (grant NAG 5-8134).

APPENDIX

NUMERICAL EVALUATION OF ANALYTIC EXPRESSIONS

The present work yields somewhat complicated analytic expressions for the separation between two magnetic field lines in two-component turbulence (§ 4.1), which are interpreted in § 4.2. We found it useful to verify that interpretation by numerically evaluating the integrals in equations (26), (27), (54), and (55) with the MATHEMATICA program (Wolfram Research, Inc.) for some special cases. Those results, plotted in Figures 5 and 6, are found to agree with the interpretation of the analytic expressions in § 4.2. In contrast, the comparison in Figures 7 and 8 with numerical simulations, which do not incorporate the analytic theory in any way, is an independent test of the validity of the analytic theory itself and its underlying assumptions.

For the numerical evaluation of analytic expressions, the following power spectra were used:

$$P_{xx}^{\rm slab}(k_z) = P_{yy}^{\rm slab}(k_z) \propto \frac{1}{\left(1 + k_z^2/k_{0z}^2\right)^{5/6}}, \tag{A1}$$

$$A(k_\perp) \propto \frac{1}{(1 + k_\perp^2/k_{0\perp}^2)^{7/3}}. \tag{A2}$$

These forms roll off to a constant at low k, and far above k_{0z} or $k_{0\perp}$ they follow a Kolmogorov law, with the omnidirectional power spectrum (OPS) varying as $k^{-5/3}$. To see this, note that for slab (one-dimensional) fluctuations the OPS is simply $P_{xx}^{\rm slab} + P_{yy}^{\rm slab}$, which has the correct dependence, and for two-dimensional fluctuations at a given magnitude $k_\perp$, the OPS $\propto k_\perp(P_{xx}^{\rm 2D} + P_{yy}^{\rm 2D}) = k_\perp^3 A$, which varies as $k_\perp^{-5/3}$ for large $k_\perp$. However, we stress that the results described in the main text do *not* require power spectra of these specific forms.

For convenience, B_0, ℓ_c, $k_{0\perp}$, and $\ell_\perp$ were all set to 1. Effectively, the calculations are for B in units of B_0, and x and z in units of $\ell_\perp$ and ℓ_c, respectively. For the slab turbulence spectrum of equation (A1), setting $\ell_c = 1$ implies that $\ell_z = 1/k_{0z} = 1.339$, and for the two-dimensional spectrum of equation (A2), $\ell_\perp = 1$ implies an ultrascale $\tilde{\lambda} = 0.577$. Figure 5 used $X_0 = 0.1$. For Figure 5*a*, the slab and two-dimensional turbulence energies were set to $\langle b^2\rangle^{\rm slab} = 7.07\times10^{-7}$ and $\langle b^2\rangle^{\rm 2D} = 7.5\times10^{-9}$, yielding $D_\parallel^{\rm slab} = 3.54\times10^{-7}$ and $D_\perp^{\rm 2D} = 3.54\times10^{-5}$, for a random walk dominated by the two-dimensional component. For Figures 5*b* and 6, the only difference was that the slab energy (i.e., $\langle b^2\rangle^{\rm slab}$) was set to 0.01, or 1.41×10^4 times stronger, for $D_\perp^{\rm slab} = 5\times10^{-3}$, so that slab turbulence dominates the random walk. These values were chosen for clarity, to separate the various physical regimes, and not to correspond to any specific physical situation such as the solar wind.

Using MATHEMATICA, we first directly calculated $\langle\Delta x^2\rangle_{\rm slab}$ for various values of Δz and then iteratively calculated $\langle\Delta x^2\rangle$ and $D_\perp$. Next D_{sx} and D_{sy} were calculated iteratively and simultaneously by a secant method (using *FindRoot*). Care was required to ensure precision and accuracy fine enough to yield good results yet coarse enough to allow the integrals and iterations to converge.

REFERENCES

Barge, P., Millet, J., & Pellat, R. 1984, ApJ, 284, 817
Barghouty, A. F., & Jokipii, J. R. 1996, ApJ, 470, 858
Batchelor, G. K. 1953, The Theory of Homogeneous Turbulence (Cambridge: Cambridge Univ. Press)
Bieber, J. W., Matthaeus, W. H., Smith, C. W., Wanner, W., Kallenrode, M.-B., & Wibberenz, G. 1994, ApJ, 420, 294
Bieber, J. W., Wanner, W., & Matthaeus, W. H. 1996, J. Geophys. Res., 101, 2511
Cane, H. V., Richardson, I. G., von Rosenvinge, T. T., & Wibberenz, G. 1994, J. Geophys. Res., 99, 21429
Cane, H. V., Wibberenz, G., Richardson, I. G., & von Rosenvinge, T. T. 1999, Geophys. Res. Lett., 26, 565
Chandran, B. D. G. 2000, ApJ, 529, 513
Corrsin, S. 1959, in Advances in Geophysics, Volume 6: Atmospheric Diffusion and Air Pollution, ed. F. Frenkel & P. Sheppard (New York: Academic), 161
Erdős, G., Balogh, A., & Kóta, J. 1997, Adv. Space Res., 19, 843
———. 1999, in Plasma Turbulence and Energetic Particles in Astrophysics, ed. M. Ostrowski & R. Schlickeiser (Kraków: Univ. Jagiellonski), 161
Fisk, L. A. 1996, J. Geophys. Res., 101, 15547
Giacalone, J., Jokipii, J. R., & Mazur, J. E. 2000, ApJ, 532, L75
Goldreich, P., & Sridhar, S. 1997, ApJ, 485, 680
Gray, P. C., Pontius, D. H., Jr., & Matthaeus, W. H. 1996, Geophys. Res. Lett., 23, 965
Isichenko, M. B. 1991a, Plasma Phys. Controlled Fusion, 33, 795
———. 1991b, Plasma Phys. Controlled Fusion, 33, 809
Jokipii, J. R. 1966, ApJ, 146, 480
———. 1973, ApJ, 183, 1029
———. 1987, ApJ, 313, 842
Jokipii, J. R., & Coleman, P. J. 1968, J. Geophys. Res., 73, 5495
Jokipii, J. R., Kóta, J., & Giacalone, J. 1993, Geophys. Res. Lett., 20, 1759
Jokipii, J. R., & Parker, E. N. 1968, Phys. Rev. Lett., 21, 44
———. 1969, ApJ, 155, 777
Jones, F. C., Jokipii, J. R., & Baring, M. G. 1998, ApJ, 509, 238
Kadomtsev, B. B., & Pogutse, O. P. 1979, in Plasma Physics and Controlled Nuclear Fusion Research, Proc. 7th Int. Conf. (Vienna: IAEA), 649
Kirk, J. G., Duffy, P., & Gallant, Y. A. 1996, A&A, 314, 1010
Kóta, J., & Jokipii, J. R. 1995, Science, 268, 1024
Krommes, J. A. 1978, Prog. Theor. Phys. Suppl., 64, 137
Kunow, H., et al. 1995, Space Sci. Rev., 72, 397
Lithwick, Y., & Goldreich, P. 2001, ApJ, 562, 279
Maron, J., Chandran, B. D. G., & Blackman, E. 2004, Phys. Rev. Lett., 92, 045001
Matthaeus, W. H., & Goldstein, M. L. 1982, J. Geophys. Res., 87, 6011
Matthaeus, W. H., Goldstein, M. L., & Roberts, D. A. 1990, J. Geophys. Res., 95, 20673
Matthaeus, W. H., Gray, P. C., Pontius, D. H., Jr., & Bieber, J. W. 1995, Phys. Rev. Lett., 75, 2136
Matthaeus, W. H., Smith, C. W., & Bieber, J. W. 1999, in AIP Conf. Proc. 471, Solar Wind Nine, ed. S. Habbal, R. Esser, J. V. Hollweg, & P. A. Isenberg (Woodbury: AIP), 511
Mazur, J. E., Mason, G. M., Dwyer, J. R., Giacalone, J., Jokipii, J. R., & Stone, E. C. 2000, ApJ, 532, L79
McComb, W. D. 1990, The Physics of Fluid Turbulence (Oxford: Clarendon)
McKibben, R. B., Simpson, J. A., Zhang, M., Bame, S., & Balogh, A. 1995, Space Sci. Rev., 72, 403
Moraal, H. 1976, Space Sci. Rev., 19, 845
Parker, E. N. 1965, Planet. Space Sci., 13, 9
Press, W. H., Teukolsky, S. A., Vetterling, W. T., & Flannery, B. P. 1992, Numerical Recipes in FORTRAN: The Art of Scientific Computing (Cambridge: Cambridge Univ. Press)
Rax, J. M., & White, R. B. 1992, Phys. Rev. Lett., 68, 1523
Rechester, A. B., & Rosenbluth, M. M. 1978, Phys. Rev. Lett., 40, 38
Reinecke, J. P. L., McDonald, F. B., & Moraal, H. 2000, J. Geophys. Res., 105, 27439
Ruffolo, D., Matthaeus, W. H., & Chuychai, P. 2003, ApJ, 597, L169
Sagdeev, R. Z., Usikov, D. A., & Zaslavsky, G. M. 1988, Nonlinear Physics: From the Pendulum to Turbulence and Chaos (Chur: Harwood)
Salu, Y., & Montgomery, D. C. 1977, Phys. Fluids, 20, 1
Sanderson, T. R., Marsden, R. G., Wenzel, K.-P., Balogh, A., Forsyth, R. J., & Goldstein, B. E. 1995, Space Sci. Rev., 72, 291
Smilon, P. L., & Sudan, R. N. 1989, ApJ, 336, 442
Simnett, G. M., Sayle, K. A., Tappin, S. J., & Roelof, E. C. 1995, Space Sci. Rev., 72, 327
Simpson, J. A., et al. 1995, Science, 268, 1019
Skilling, J., McIvor, I., & Holmes, J. A. 1974, MNRAS, 167, 87P
Zaslavsky, G. M., & Chirikov, B. V. 1972, Soviet Phys. Uspekhi, 14, 549
Zimbardo, G., Veltri, P., & Malara, F. 1984, J. Plasma Phys., 32, 141

GEOPHYSICAL RESEARCH LETTERS, VOL. 32, L03S02, doi:10.1029/2004GL021492, 2005

Relativistic solar neutrons and protons on 28 October 2003

John W. Bieber, John Clem, Paul Evenson, and Roger Pyle
Bartol Research Institute, University of Delaware, Newark, Delaware, USA

David Ruffolo
Department of Physics, Mahidol University, Bangkok, Thailand

Alejandro Sáiz[1]
Department of Physics, Chulalongkorn University, Bangkok, Thailand

Received 14 September 2004; revised 14 October 2004; accepted 17 November 2004; published 11 January 2005.

[1] The solar cosmic ray event associated with the X17.2 class flare of 28 October 2003 was unusual in several respects: (1) Several high-latitude neutron monitors observed a large, highly anisotropic spike at event onset. (2) The earliest onset was detected by stations viewing towards the anti-Sunward hemisphere. (3) The event displayed an extremely slow, protracted decay. (4) The near-equatorial monitor in Tsumeb, Africa recorded a small increase consistent with a solar neutron event ≈7 minutes prior to the onset at high latitudes. We analyze these signals and infer that relativistic solar neutrons were emitted over a duration of ≈9 minutes, starting ≈7 minutes before the main injection of relativistic protons. **Citation:** Bieber, J. W., J. Clem, P. Evenson, R. Pyle, D. Ruffolo, and A. Sáiz (2005), Relativistic solar neutrons and protons on 28 October 2003, *Geophys. Res. Lett.*, *32*, L03S02, doi:10.1029/2004GL021492.

1. Introduction

[2] Relativistic solar cosmic rays provide a vital observational basis for understanding acceleration processes near the Sun. When a high flux of solar nucleons with energy greater than a few hundred MeV strikes Earth's atmosphere, the nuclear byproducts cascade to Earth's surface resulting in a "ground level enhancement" (GLE). A distributed network of neutron monitors, such as the *Spaceship Earth* observing network [*Bieber et al.*, 2004], provides an effective means of studying the angular distribution and energy spectrum of these energetic solar particles.

[3] The extreme solar activity of October–November 2003 produced 3 GLEs, with onsets occurring on 28 October, 29 October, and 2 November. This *Letter* concerns the first and largest of these. We present an overview of neutron monitor observations and point out a number of unusual features of this event. We propose that relativistic solar neutrons were emitted at the start of the event. We also model the main phase of the event to determine the solar proton release time and injection function.

[1]Also at Department of Physics, Mahidol University, Bangkok, Thailand.

0094-8276/05/2004GL021492$05.00

2. An Unusual GLE

[4] Figure 1 presents count rates measured by selected stations of the *Spaceship Earth* neutron monitor network as a function of time on 28 October 2003. This GLE was associated with an X17.2 solar flare located at S16 E08 that reached maximum soft X-ray intensity at 11:10 UT. The time profiles in Figure 1 display several unusual features.

[5] First, a few stations observed a large, narrow spike at event onset. McMurdo observed the largest spike, a 43% increase over the pre-event Galactic background. Most stations did not observe such a spike, or saw a smaller feature, indicating that the particles causing the spike were extremely anisotropic. An expanded view of the spikes appears in Figure 2b. Note that all *Spaceship Earth* neutron monitors are at polar locations and have essentially identical energy responses; any differences in count rates can be attributed to the different viewing directions.

[6] Second, the earliest arriving particles were detected by stations observing the anti-Sunward hemisphere. At high latitudes the earliest onsets were at Norilsk (11:14 UT) and Cape Schmidt (11:13 UT), which were respectively viewing towards GSE longitudes of 127° and 192°, the latter being almost directly anti-Sunward!

[7] Third, the event displayed an unusually slow decay. Intensities remained elevated by several percent over the pre-event background until about 06:00 UT the following day, a total of about 19 hours. In comparison, station intensities in the more typical GLE of Easter 2001 [*Bieber et al.*, 2004] declined to one-tenth their peak value after only 4 hours. The 28 October 2003 GLE persisted until the coronal mass ejection (CME) shock associated with the X17.2 flare arrived at Earth, resulting in the largest Forbush decrease of the present solar cycle. (The decrease continues beyond the time shown in Figure 1, ultimately reaching 27% at South Pole.)

[8] Fourth, as shown in Figures 1b and 2a, the near-equatorial neutron monitor in Tsumeb, Namibia observed a small but clear increase in count rate beginning at 11:06 UT and lasting for ~9 minutes. (Note that the ordinate in these panels is excess count rate; the increase at Tsumeb amounts to 3–4% above the pre-event background.) This precursor increase seen at a high-altitude (1240 m) station near the subsolar point (zenith angle 8.4°) is reminiscent of earlier solar neutron events detected by neutron monitors [*Chupp et al.*, 1987; *Shea et al.*, 1991b]. The presence of direct

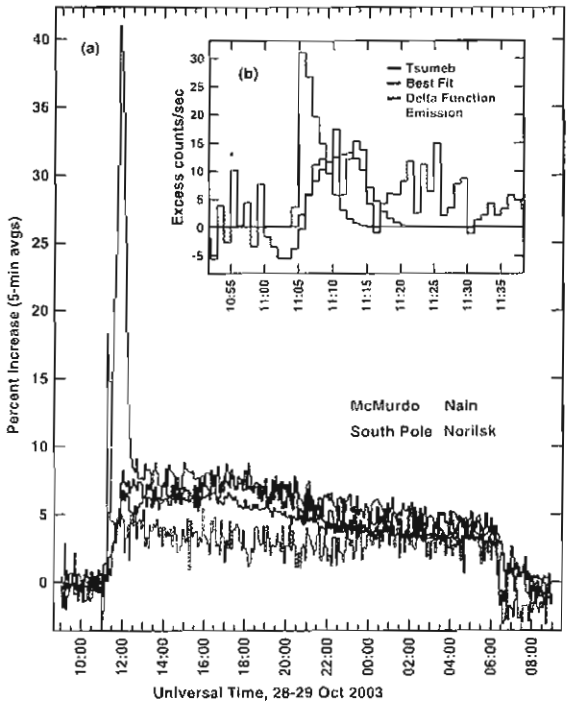

Figure 1. (a) Overview of the 28 October 2003 ground level enhancement (GLE), as observed by four selected stations of *Spaceship Earth*. Count rates are expressed as a percent increase over the pre-event Galactic background. All data are 5-minute averages corrected to standard pressure (760 mm Hg) using an assumed solar particle absorption length of 100 g cm^{-2}. (b) Excess count rate observed by the neutron monitor in Tsumeb, Africa (red), compared with our best fit for extended neutron emission at the Sun (blue) and expectation for δ-function emission at the Sun (green).

neutrons at Tsumeb in this event was previously noted by *Plainaki et al.* [2004].

3. Modeling of the Neutron Event

[9] During intense solar events, accelerated protons and nuclei produce high energy neutrons through inelastic collisions in the solar atmosphere. These (uncharged) neutrons follow a straight line path from the emission point to Earth undisturbed by magnetic fields, arriving before direct protons from the same event. If the neutron emission time is very short compared to the propagation time to Earth, the observed time profile of the neutron monitor allows a direct time-of-flight measurement of the energy spectrum. However, there have been reported cases of extended emission lasting hours, while others may be as brief as a minute [*Chupp*, 1995; *Muraki and Shibata*, 1995, and references therein].

[10] The nuclear processes responsible for solar neutron emission also generate high energy gamma rays [*Lingenfelter and Ramaty*, 1967], which can provide a key proxy for the neutron emission profile. Unfortunately, we have not obtained such measurements at the time of writing.

[11] On 28 October 2003 at 11:06 UT the Tsumeb neutron monitor recorded a 3–4 percent increase that began 7 minutes before the onset of charged particle GLE signals and persisted for roughly 9 minutes. The Tsumeb monitor is an 18-NM-64 instrument located in Namibia at 17.58°E, 19.2°S (9.12 GV vertical cutoff rigidity), with 1240 m elevation resulting in average atmospheric pressure of 660 mm Hg. Using a Monte Carlo code [*Clem and Dorman*, 2000; *Fasso et al.*, 2001] to simulate high energy and nuclear transport through the atmosphere and through an 18-NM-64 neutron monitor, the Tsumeb yield function for solar neutrons was calculated. The resulting Tsumeb yield function is shown in Figure 3 (red squares) along with related quantities.

[12] The black curve in Figure 3 is *Chupp*'s [1990] spectrum derived for the 2 June 1982 event

$$Q = 1.293 \times 10^{30} E_n^{3/8} \exp\left[-(E_n/0.016)^{1/4}\right], \qquad (1)$$

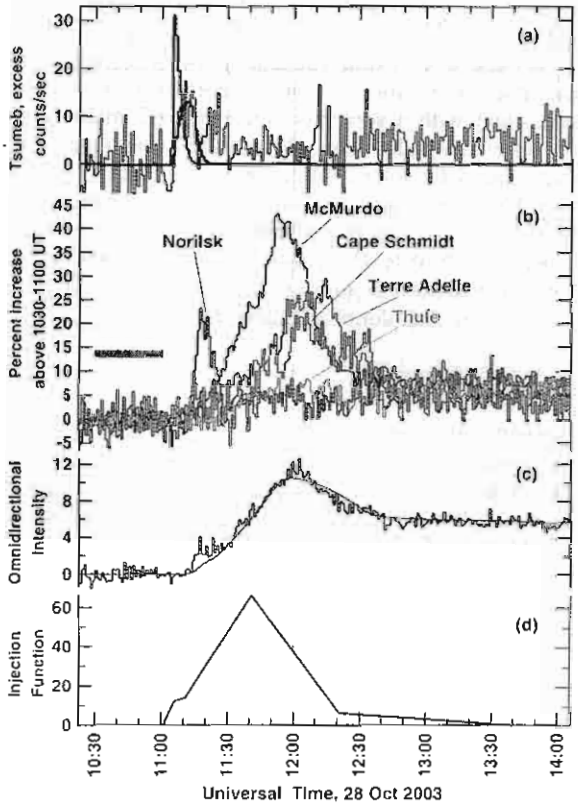

Figure 2. (a) Excess count rate at Tsumeb neutron monitor with fits as in Figure 1b. (b) Expanded view of the spikes observed by several stations at the beginning of the GLE. Station intensities are expressed as a "percent increase" over the pre-event Galactic background during a normalization interval 10:30–11:00 UT indicated by the horizontal bar. These are 1-minute data corrected to standard pressure. (c) Directionally averaged intensity (blue) at polar neutron monitors and model fit (red) to main peak. (d) Model injection function (solar time) of relativistic solar protons, optimized to fit intensity and weighted anisotropy during and after the main peak, for a closed magnetic loop of length 4.2 AU.

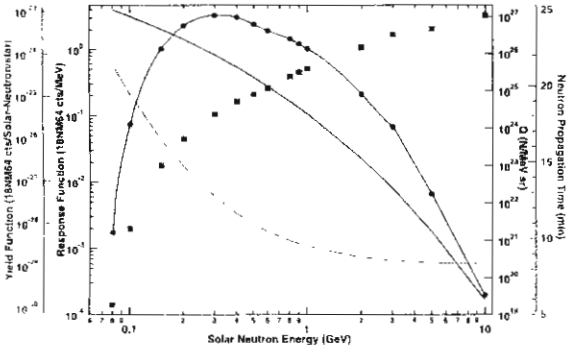

Figure 3. Tsumeb 18-NM-64 yield function versus energy for neutrons arriving 8.4° from zenith (red squares), *Chupp*'s [1990] exponential spectrum (black curve), Tsumeb response function (blue), and propagation time of a neutron from the Sun to 1 AU (green).

where Q is the spectrum in units of (sr MeV)$^{-1}$, and E_n is neutron energy in MeV. We found that simple linear scaling of this spectrum provides a good description of the 28 October 2003 event. The blue curve in Figure 3 is the Tsumeb response function (product of yield function and spectrum), and the green curve shows the propagation time of a neutron from the Sun to 1 AU. For a given emission time profile, we can derive the expected count rate profile by integrating the response function in time delayed segments based on propagation time to Earth.

[13] In order to derive start time and emission duration, a least squares fit was performed assuming the emission time profile can be represented by a boxcar function. The fit has three free parameters: the normalization, onset time, and duration. The result of this fit is shown in Figures 1b and 2a. The blue line represents the best fit with emission onset at the Sun at 10:56:30 ST +1 minute ("ST" is Solar Time, and refers to the Universal Time of an event at the Sun) and an emission duration of 8.7 minutes. The scaling factor (relative to *Chupp*'s [1990] spectrum) is 0.93. The model represents the data well.

[14] The green curve in Figures 1b and 2a illustrates the count rate profile expected for an instantaneous emission with the same normalization and start time determined from the three parameter fit. This is clearly inconsistent with the data. We tried other neutron spectral shapes (power law variations) and found that the emission duration time did not vary by more than ~1 minute.

4. Why Did the First Particles Arrive From Anti-Sunward?

[15] Given strong indications that relativistic solar neutrons were detected in the 28 October GLE, we considered the possibility that neutron decay protons (NDP) [*Ruffolo*, 1991; *Shea et al.*, 1991a] might account for the early onset and anomalous arrival directions observed at Norilsk and Cape Schmidt. Neutrons decaying locally onto a (hypothetical) near azimuthal field will have an initial pitch angle near 90°. One-half gyroperiod after they decay, they will be moving back toward the Sun and could in principal be detected by stations viewing anti-Sunward.

[16] However the NDP hypothesis encounters difficulties on two grounds. First, one would expect NDPs to onset at the same time as direct neutrons, but the Cape Schmidt (proton) onset followed the Tsumeb (neutron) onset by 7 minutes. Second, we modeled NDP intensity using the neutron spectrum derived above, and we obtained a sea level NDP signal less than 1%, more than 20 times smaller than the increase observed at Norilsk.

[17] A second hypothesis for the anomalous arrival direction of the first particles is that Earth was located inside a closed magnetic loop at event onset. If the first injection of particles was on the far leg (relative to Earth) of the loop, then the far-leg particles would move past 1 AU, loop back, and be observed at Earth coming from anti-Sunward. Indeed, even without the anti-Sunward spike, trapping of particles in a magnetic loop might be hypothesized to account for the unusually slow decay of the event. Anti-Sunward streaming in a loop geometry explains various unusual features of the 22 October 1989 GLE [*Ruffolo et al.*, 2004] and is observed rather commonly in lower energy ions [*Richardson and Cane*, 1996]. The problem with this scenario is a lack of independent evidence that Earth was in a closed magnetic loop at event onset. Further analysis is needed to answer the question posed in the title of this section.

5. Modeling Relativistic Solar Protons

[18] While the excess counts of the Tsumeb neutron monitor can be attributed to solar neutrons, the GLE at high latitude stations is attributed to relativistic solar protons. Given the uncertain origin of the initial spike from the anti-Sunward hemisphere, we do not attempt quantitative modeling of those data at present. Instead, we concentrate on the later anisotropic spike observed at McMurdo, Cape Schmidt, and Terre Adelie (Figure 2b).

[19] We first fit data from 13 neutron monitors (11 stations of the *Spaceship Earth* network supplemented by Terre Adelie and Barentsburg) to a second-order Legendre expansion about an optimal axis of symmetry taking into account bending of particle trajectories in Earth's magnetic field. The omnidirectional intensity and weighted anisotropy (standard anisotropy multiplied by intensity) are extracted as quantities to be fit by the transport model. Then we numerically solve a transport equation that takes into account pitch angle scattering and adiabatic focusing [*Ruffolo*, 1991; *Nutaro et al.*, 2001].

[20] In this analysis, we consider two types of magnetic field configurations: (1) a standard Archimedean spiral for the measured solar wind speed of approximately 800 km/s [Source: http://www.srl.caltech.edu/ACE/ASC/level2/lvl2DATA_SWEPAM.html.], and (2) a closed magnetic loop of total length $\ell = 4.2$ AU. In both models, Sun-Earth distance along the magnetic field is taken to be 1.03 AU. For the focusing length $L = -B/(dB/dz)$, where B is magnetic field strength and z is distance along the magnetic field, the loop model uses the functional form

$$\frac{1}{L} = \frac{2\pi}{\ell}\cot\left(\frac{\pi z}{\ell}\right) \qquad (2)$$